University of Houston
Alaska University Transportation Center

Impact of Embedded Carbon Fiber Heating Panel on the Structural/Mechanical Performance of Roadway Pavement

Zhaohui "Joey" Yang
Xiaoyu Zhang
School of Engineering, University of Alaska Anchorage
Gangbing Song
Mithun Singla
Divendra Patil
Dept. of Mechanical Engineering, University of Houston

December 2012

Alaska University Transportation Center
Duckering Building Room 245
P.O. Box 755900
Fairbanks, AK 99775-5900

University of Houston
Cullen College of Engineering
N207 Engineering Building 1
Houston, TX 77204-4006

INE/ AUTC 12.39

REPORT DOCUMENTATION PAGE

Form approved OMB No.

1. AGENCY USE ONLY (LEAVE BLANK)	2. REPORT DATE	3. REPORT TYPE AND DATES COVERED
	December 2012	Final Report (7/1/2011-12/31/2012

4. TITLE AND SUBTITLE

Impact of Embedded Carbon Fiber Heating Panel on the Structural/ Mechanical Performance of Roadway Pavement

5. FUNDING NUMBERS

AUTC #510022
DTRT06-G-0011

6. AUTHOR(S)
Zhaohui Yang, Xiaoyu Zhang, Gangbing Song, Mithun Singla, Divendra Patil

7. PERFORMING ORGANIZATION NAME(S) AND ADDRESS(ES)
Alaska University Transportation Center
P.O. Box 755900
Fairbanks, AK 99775-5900

8. PERFORMING ORGANIZATION REPORT NUMBER

INE/AUTC 12.39

9. SPONSORING/MONITORING AGENCY NAME(S) AND ADDRESS(ES)
Research and Innovative Technology Administration (RITA) (USDOT)
1200 New Jersey Ave, SE, Washington DC 20590
University of Houston, Cullen College of Engineering
N207 Engineering Building 1, Houston, TX 77204-4006

10. SPONSORING/MONITORING AGENCY REPORT NUMBER

11. SUPPLENMENTARY NOTES

12a. DISTRIBUTION / AVAILABILITY STATEMENT

No restrictions

12b. DISTRIBUTION CODE

13. ABSTRACT (Maximum 200 words)

An ongoing collaborative research project is helping find more cost-effective and sustainable de-icing solutions to benefit a wide variety of transportation infrastructure users. Partnering with the AUTC and the University of Houston, researcher Zhaohui Yang of UAA plans to test a carbon fiber tape (CFT) based de-icing technology in hopes of offering an environmentally-friendly, anti-corrosive, cost-effective de-icing technology that can improve transportation safety. This new de-icing technology is potentially applicable to bridge decks, road sections susceptible to icing, airport runways, street crossings and frequently used sidewalks in urban areas in Alaska and other cold regions.

Cold regions like Alaska suffer serious transportation system safety problems in the winter months. South central Alaska—Anchorage in particular—is susceptible to a large number of icing events due to frequent freeze/thaw cycles in the winter season. This creates ice on sidewalks, pavement and bridge decks that poses a significant safety risk to pedestrians, travelers/commuters, and commercial drivers alike. Black ice, a thin shiny layer of ice with a slick surface, is of particular concern because of its near invisibility o drivers, pilots and pedestrians.

14- KEYWORDS: Carbon fibers (Rbmdxfc), Pavement performance (Estyp), Asphalt pavements (Pmrcppbmb)

15. NUMBER OF PAGES

16. PRICE CODE

N/A

17. SECURITY CLASSIFICATION OF REPORT	18. SECURITY CLASSIFICATION OF THIS PAGE	19. SECURITY CLASSIFICATION OF ABSTRACT	20. LIMITATION OF ABSTRACT
Unclassified	Unclassified	Unclassified	N/A

Table of Content

List of Figures

List of Tables

Acknowledgment

The research reported herein was supported by the Alaska University Transportation Center (AUTC Project # 510022) and performed by the Department of Civil Engineering at University of Alaska Anchorage (UAA) and the Department of Mechanical Engineering at the University of Houston (UH).

Dr. Zhaohui Yang, Associate Professor of Civil Engineering at UAA, was the Principal Investigator. Mr. Xiaoyu Zhang, former graduate student of UAA, Mr. Benjamin Still, Ms. Xiaoxuan Ge, graduate students of UAA have worked as Research Assistant on this project. Dr. Gangbing Song, Professor of Mechanical Engineering at University of Houston (UH) lead the experiments conducted at UH. Mr. Mithun Singla, former Ph.D. candidate, and Mr. Devendra Patil, Ph.D. candidate at UH have worked as Research Assistant in this project.

Abstract

In cold regions, snow and ice cause serious safety problems to transportation systems. Traditionally, deicing has been accomplished by mechanical, chemical, and thermal means. However, these methods cause problems such as damage to pavement, pollution in the environment, and corrosion to vehicles and reinforcing steel in concrete. These methods are also expensive. A new type of deicing system that uses commercially available carbon fiber tape (CFT) is proposed and validated as very effective in deicing/anti-icing applications in Phase I of this study as previously reported. Phase II study focuses on the issues raised during field experiments of the CFT heating panel embedded in concrete sidewalk for deicing. This report presents the results obtained from a comprehensive study of these issues including induced current, automatic control algorithms, impact of the CFT embedment on the structural integrity of concrete slabs, survivability of the CFT during concrete cracking, and field performance observation. Computer simulation was conducted on the level of current induced by the CFT heating panel during deicing. Two automatic controllers – ON/OFF Controller and Fuzzy-logic controller – were implemented at the UAA test site and their performance was monitored and analyzed. Laboratory experiments were conducted to investigate the embedment of CFT on the structural integrity of the concrete slab and the survivability of the CFT heating panel to the cracking of concrete slab. In the end, observation of the performance of the test sidewalk with embedded CFT heating panels was made and the results of the electrical resistance measured at the test side during the two and a half year field experiments were presented. It is concluded that effective automatic controller can be used to reduce the energy cost substantially. The current induced by the CFT heating panel system is negligible as far as corrosion is concerned. The CFT heating panel has promising long-term reliability and stability, and can survive a crack of more than a quarter inch.

Executive Summary

This report describes the results obtained from a comprehensive study on practical issues related to application of the CFT heating panel deicing system in the field. The main findings from this project are summarized below:

1. The expected induced current in the steel rebar mesh is at the level of nano Amps and its impact on corrosion is negligible.

2. Compared with the manual control, the automatic controllers such as the ON/OFF controller and Fuzzy Logic-based controller reduce the power consumption or cost by 59% and 70%, respectively. The ON/OFF controller is simple and efficient. It is recommended for field application.

3. Embedment of the CFT can provide higher strength to the concrete slab while being used as heating elements for deicing application. However use of the CFT alone for the reinforcement purpose is not recommended as the CFT can only provide very limited ductility as compared to steel rebar.

4. The uncoated CFT can survive ¼ in. wide concrete crack without sacrificing its heating capacity. It is envisioned that the CFT coated with flexible electrically insulating epoxy can survive much large cracks in concrete slabs.

5. The CFT heating panel deicing system demonstrates excellent deicing/anti-icing capability and quite stable electrical resistance during the two and a half year-long field experiment and this shows its promising long-term reliability and stability.

A provisional patent application has been filed to protect the intellectual property rights of this new deicing technology (U.S. Patent Application No. 61/699,372). It is anticipated that after large-scale field trials, the CFT heating panel-based deicing system could find applications that include, but are not limited to, sidewalks and parking lots in

urban areas, bridge decks and road sections susceptible to icing, roofs of residential and commercial buildings, and street crossings in Alaska and other cold regions.

CHAPTER 1: INTRODUCTION

1.1 Background

In cold regions, snow and ice causes serious safety problems to the transportation system. South central Alaska, particularly, Anchorage, is susceptible to a large number of icing events due to frequent freeze-thaw cycles in winter season. Icing on the sidewalk, pavement and bridge decks is posing a persistent threat to the safety of the public. In particular, a thin, shiny layer of ice with a slick surface, commonly called black ice, often forms on highway pavement and bridge decks when moisture condenses and freezes. It is difficult for motorists to discern, and therefore responsible for many accidents. There is a great need for an environment-friendly, anti-corrosion, and cost-effective deicing technology for improving the transportation safety.

With the support from the Alaska University Transportation Center (AUTC), University of Alaska Anchorage (UAA) and University of Houston, a carbon fiber tape (CFT) heating panel deicing technology has been developed and a field experiment sidewalk equipped with such deicing technology has been built on the UAA campus in September 2010 (Yang et al. 2012). A series of deicing and anti-icing experiments have been successfully conducted. Preliminary results show that the cost of deicing and anti-icing is considerably lower than other deicing technologies based on electrical resistive heating and this new technology demonstrates excellent deicing capability.

In addition, this technology does not require change in pavement material design. Its system installation is relatively simple, involving laying CFT heating panels on the lower portion of regular pavement with minimum interference to pavement or bridge deck construction. It is potentially applicable to the de-icing of bridge decks, road sections susceptible to icing, airport runways, street crossings and frequently used sidewalks in urban areas in Alaska and other broader cold regions.

However, during the pilot testing, three major questions were brought to our attention and they need to be resolved before this technology is readily applicable in the field. These questions are: 1) the impact of heating panel embedment to structural integrity of pavement/bridge decks, , 2) the reliability of the CFT heating panel including the impact of coupled thermal cycling (i.e. heating-cooling from deicing operation) and freeze-thaw cycling (due to ambient temperature fluctuations) on the electrical properties of the heating panels and the survivability of the heating panel to potential pavement cracking, and 3) the impact of electromagnetic field generated by the deicing operation on the corrosion of steel reinforcement in the pavement/bridge deck. This study aims to answer these questions before its application in the field.

1.2 Literature Review

1.2.1 Application of carbon fiber in strengthening concrete structures

Fiber reinforced polymer (FRP) composite materials have been successfully used in new construction and for the repair and rehabilitation of deteriorated structures. Carbon fiber reinforced polymers (CFRP) have shown great promises in strengthening the structures and have attracted researchers from all over the world for their properties including light-weight, high strength-to-weight and stiffness-to-weight ratios, ease of installation, resistance to electro-chemical corrosion, and versatility in fabrication. Various studies have been done in the past to investigate the effectiveness of the carbon fiber reinforcement. Studies (Shahawy et al. 1996a&b; Täljsten and Elfgren 2000) show that bonding carbon FRP laminates to the tension side of beams and slabs can considerably increase their bending and shear capacity. The corrosion resistance feature makes the FRP grids ideal reinforcement materials for concrete slabs; several studies show that near-surface CFRP grid reinforcement can greatly reduce surface cracking (e.g. Ramakrishnan 2001). Bae et al. *(*2005) conducted a study to show the effectiveness of CFRP in strengthening damaged reinforced concrete (RC) columns due to corrosion. It was concluded that CFRP wrapping will help strengthen the structure and decrease the corrosion rate.

Reliable interface bond between FRP and concrete substrate is of critical importance for external strengthening technology using FRP. Okelo et al. (2005) studied the bond strength of FRP in normal strength concrete. Different types of reinforcing bars or rebars were tested using the pullout method and it was found that the bond strength of concrete structure depends upon the Young's modulus of rebars. Malvar et al. (2003) analyzed the bond characteristics of four different types of CFRP rebars with different surface deformations embedded in lightweight concrete. It was found that small surface indentations were sufficient to yield bond strengths comparable to that of steel rebars. The pullout test provided preliminary data for development of length assessment and model validation. Cox et al. (2003) further provided computational modeling of the bonding behavior for obtaining preliminary design data for the needed cover thickness, development length, and transfer lengths. FRP has been used in different configurations to ensure the long service life of the structure.

1.2.2 Effect of thermal cycling on CFRP reinforced beams

A substantial body of knowledge related to the effects of elevated temperature cycles on material properties of Portland cement concrete has been gained for the design of nuclear reactor. Thermal cycling, even at relatively low temperatures (65°C), can have adverse effects on concrete mechanical properties. Study results (Campbell-Allan et al. 1965; Campbell-Allen and Desai 1967; Kassir et al. 1996) indicate that the compressive, tensile and bond strengths, and the modulus of elasticity of limestone concrete are considerably reduced. Naus (2005) presented a comprehensive review of the effect of elevated temperature on concrete materials and structures.

Several researchers studied the impact of freeze-thaw cycle on the mechanical properties of carbon fiber reinforced composites. For example, Dutta and Hui (1996) demonstrated that at low temperature, carbon fiber reinforced composite exhibits slightly higher stiffness, increased compressive strength and rigidity. However, freeze-thaw exposure results in reduction in the tensile strength of CFRP composites, and this may be due to a combination of moisture absorption, low temperature effects and thermal cycling effects (Wang 1986; Eckold 1994). Kaiser (1989) found that there were no detrimental effects on the overall structural performance of beams plated with carbon FRP sheets tested after 100 freeze-thaw cycles from -25° to +25°C. Baumert et al. (1996) found cold weather has no adverse effects on the structural behavior of CFRP plated beams when subject to a static load and ambient temperature of -27° to +21°C.

1.2.3 Corrosion of steel reinforcement due to induced current

When the current pass through the CFT heating panel, it generates an electromagnetic field which will in turn induce a current in the steel reinforcement placed in the pavement or bridge decks. The induced current, if significant, can accelerate the corrosion rate of steel reinforcement. The effects of magnetic field on the corrosion or dissolution of metals has been reported previously (Chiba et al. 1994; Sasada and Akira 2000 Sato et al. 2002; Sueptitz et al. 2010). There are two ways that electromagnetic current influences corrosion: (1) D/C current (under applied or permanent magnetic fields) and A/C electric current, which creates electromagnetic fields through Lenz's Law, may influence magnetocorrosion (Jackson et al. 2007); and (2) A/C current has the potential to strip the protective passive layer from materials and greatly accelerate corrosion. For example, Osella et al. (1998) studied the current induced by geomagnetic storms on buried pipelines; their results indicate that geomagnetic effects can introduce significant disturbance on buried pipelines, increasing their risk of corrosion and potentially reducing their safe useful life.

1.2.4 Summary

A literature review was conducted regarding these issues raised in applying CFT heating panel in deicing applications. CFRP was used as reinforcing material for improving structural member strength either externally or internally in the form of sheets and rebars. The impact of thermal cycles to the mechanical properties of carbon fiber reinforced composites was investigated. These thermal cycles include those above and below the water freezing point. Almost all studies were to do with carbon fiber sheets or rebars. Little study is directed toward to composites with embedded carbon fiber tape (CFT). How well is the bonding between the concrete and the CFT with or without coating? How will the embedded CFT impact the integrity or flexural behavior of the concrete slab? In addition, very limited studies can be found on the induced current in concrete steel rebars and its impact on the corrosion of steel rebars.

1.3 Study Objective

The objective of this project is to develop an innovative, environment-friendly, anti-corrosion and cost-effective deicing technology that is readily applicable in the maintenance and operation of the transportation infrastructure by resolving the major issues identified above. A combination of numerical simulation and laboratory/field experiments will be used. The pullout and bending tests will be performed to study the bonding between the concrete and the CFT and assess the impact of the embedded CFT on the structural integrity or flexural behavior of Portland cement concrete surface pavement. Theoretical analyses and laboratory/field experiments will be performed to assess the impact of electromagnetic field created by the heating panel on the corrosion of the steel reinforcement. Field observation and property measurement of the CFT heating panels in the outdoor experiment facility will be conducted to evaluate the impact of coupled thermal and freeze-thaw cycles on the reliability of the CFT heating panel deicing technology. In addition, various automatic control algorithms will be studied to improve the operating cost and make this deicing system a more attractive deicing alternative.

1.4 Scope of Work

The essential tasks of this project include:

1) Assessing the impact of the CFT embedment on the structural integrity of the pavement and field assessment of the deicing system in laboratory;

2) Evaluating the reliability of the deicing system under harsh thermal cycles from deicing operations and freeze-thaw cycling due to ambient temperature fluctuations and the survivability of the heating panel to potential pavement cracking;

3) Conducting theoretical, laboratory and field study of the CFT heating panel-induced current and potential impact on the corrosion of the rebars; and

4) Investigating various automatic control algorithms on the operating cost of the deicing system.

1.5 Organization of This Report

This report is divided into the following chapters:

5) Chapter 1 introduces the background, presents literature review, study objectives, and the scope of work;

6) Chapter 2 presents a study of the induced current in the rebars;

7) Chapter 3 presents automatic control algorithms developed for the CFT heating panel deicing technology and assess their efficiency on improving the operating cost;

8) Chapter 4 analyzes structural integrity of concrete slab embedded with CFTs by conducting 3- and 4-point bending tests;

9) Chapter 5 evaluates the reliability of the CFT heating panel under harsh thermal cycles and assess the survivability of the CFT heating panel to potential pavement cracking; and

10) Chapter 6 summarizes the content and presents conclusions of this study, and discusses suggestions for future study.

CHAPTER 2: CFT HEATING PANEL INDUCED CURRENT

2.1 Introduction

As mentioned in the previous chapter, the AC current passing the CFT heating panel may generate an electromagnetic field, which in return could induce a current in the steel rebar and hence accelerate the corrosion process. Figure 2.1 present a snapshot of the sidewalk construction site, from which the CFT heating panel and the steel rebar mesh are visible. The vertical distance between the CFT heating panel and the steel rebar is 1 in. The width of the CFT strips is 2 in.; #6 and #11 steel bars were used. This chapter presents the induced current results obtained from a field measurement and computer simulations.

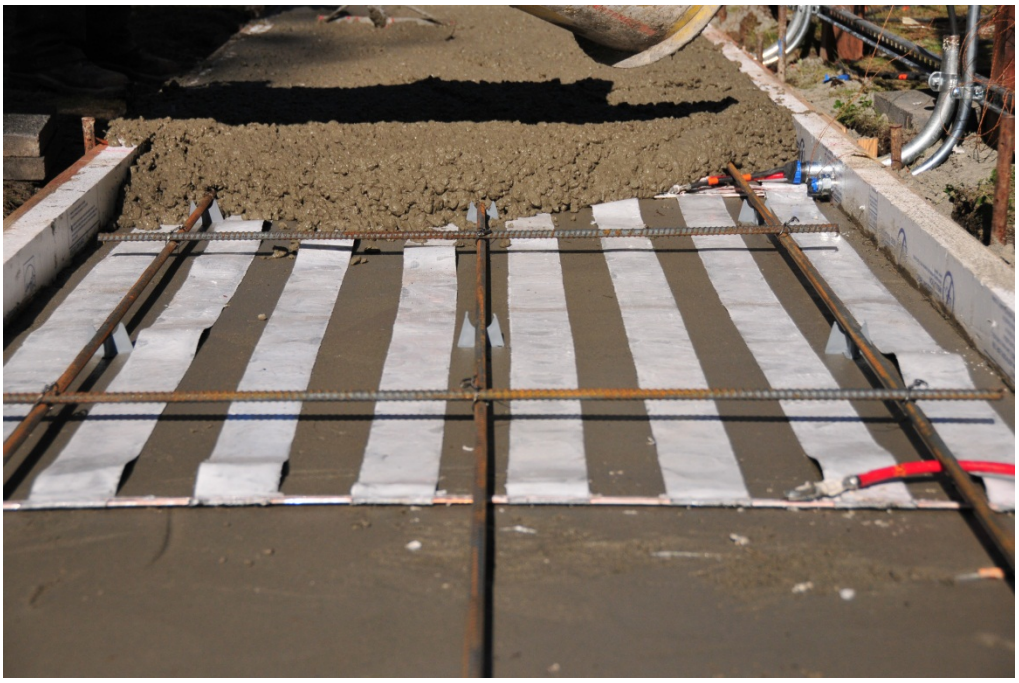

Figure 2.1 A snapshot of the sidewalk construction site showing the CFT heating panel and the steel rebar mesh

2.2 Field measurement

A simple test was designed to measure the current in the steel rebar mesh induced by the embedded CFT heating panel (see Figure 2.1). Figure 2.2 shows a schematic of the heating panel embedded in the concrete slab. There are eight CFT strips of 2” wide laid out in parallel on each panel. A 24 V 60 Hz voltage was applied to the heating panel to warm up the concrete slab surface, resulting in an AC current of 2.5 A through each CFT strip. A steel rebar frame was constructed with conductive joints and laid upon the concrete surface, as illustrated in Figure 2.3. We used a Keithly 2400 Sourcemeter with AC current resolution of 10 μA to measure the current

induced into the steel rebar frame, both with and without powering the CFT heating panel. Comparison of the induced current with and without powering the CFT heating panel showed no measureable difference in the induced current, indicating any change in the induced current was below the 10 μA resolution of the Sourcemeter.

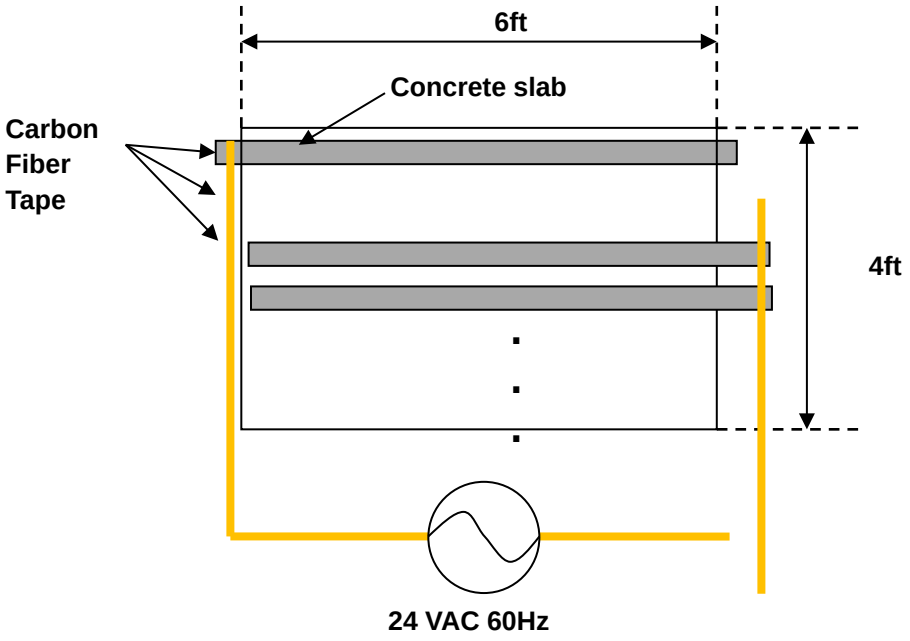

Figure 2.2 Schematic of the CFT Heating Panel in Concrete Slab

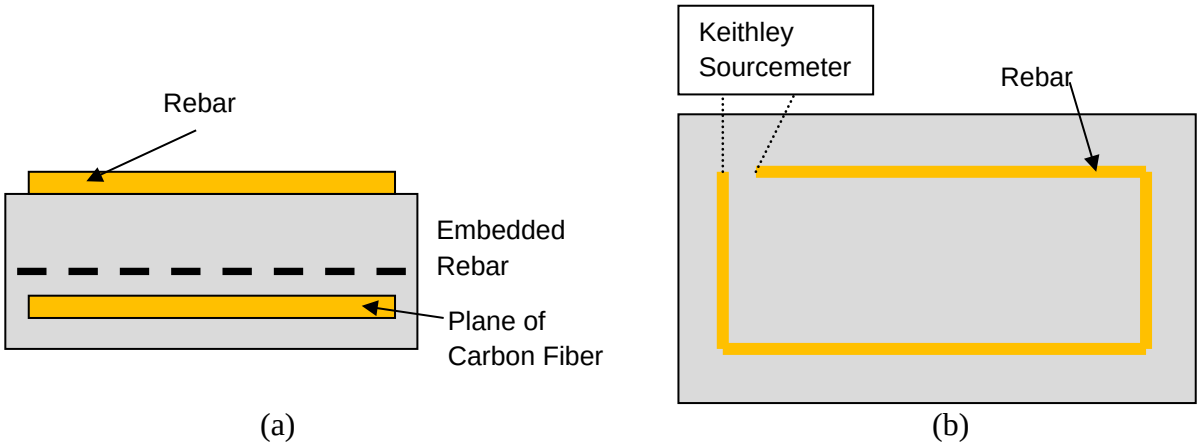

Figure 2.3: Experiment Setup for Induced Current Measurement: (a) Side View and (b) Top View

2.3 Computer Simulation

2.3.1 Model setup

Based on the sidewalk deicing experiment, a computer model consisting of a concrete block with embedded CFT tape and steel rebar is built for electromagnetic field and induced current simulation. A few important factors which may impact the induced current are analyzed by using electromagnetic simulation software based on the FDTD approach in the time domain. The induced current depends on the vertical distance (d) and the cross angle (α) between the CFT and the steel rebars. Figure 2.4 shows a schematic of the simulated system and Figure 2.5 show a case where α is zero (parallel). The key features of the setup are described as follows:

1) The size of the concrete block is 1000 cm × 1000 cm × 70 cm and its relative permittivity is assumed to be 8.
2) The length and the width of the CFT in the concrete is 3 m and 2.5 cm, respectively.
3) The CFT is powered by an alternating current (AC) source with a voltage of 24 V and a frequency of 60 Hz.
4) The steel rebar has a length of 3 m and a diameter of 1.9 cm (or #6 bar); and
5) The vertical distance d and cross angle can be adjusted as needed.

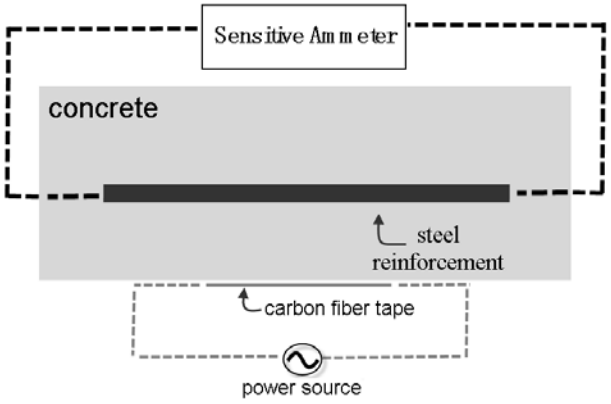

Figure 2.4 Schematic of the electromagnetic simulation setup

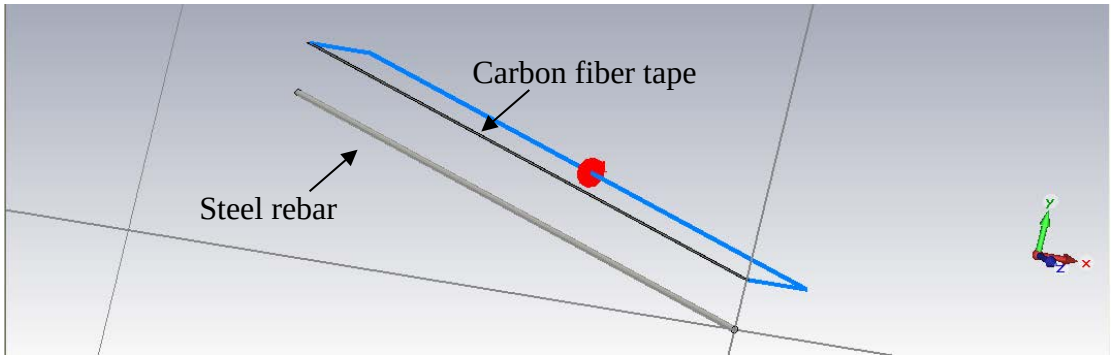

Figure 2.5 Schematic of the CFT and the steel rebar with zero cross angle

2.3.2 Simulation Results

Assuming a constant d of 2.5 cm (1 in.), the cross angle can be adjusted to simulate the different segment of steel rebars in the mesh. When the cross angle is zero (the CFT and rebar are parallel to each other), the peak induced current is 4.31 nA. Furthermore, the current distributes quite uniformly along the rebar (see Figure 2.6). When the cross angle is 90° (the CFT and rebar are perpendicular to each other), the peak induced current is 1.78 nA (see Figure 2.7). In this case, however, the current distributes unevenly along the rebar.

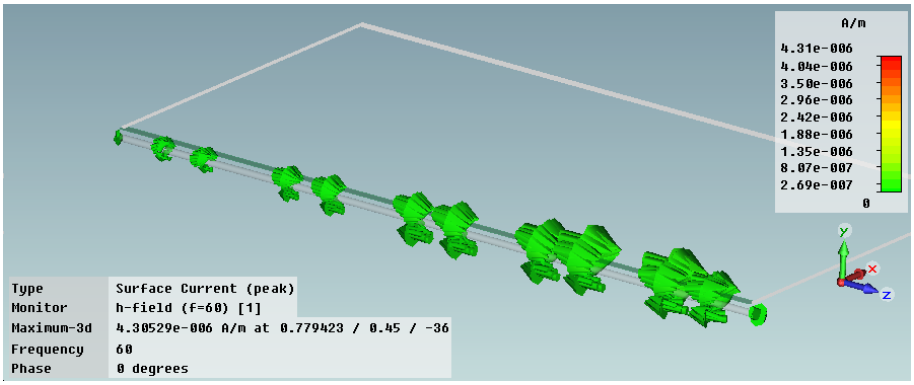

Figure 2.6 Induced current distribution for the zero cross angle case

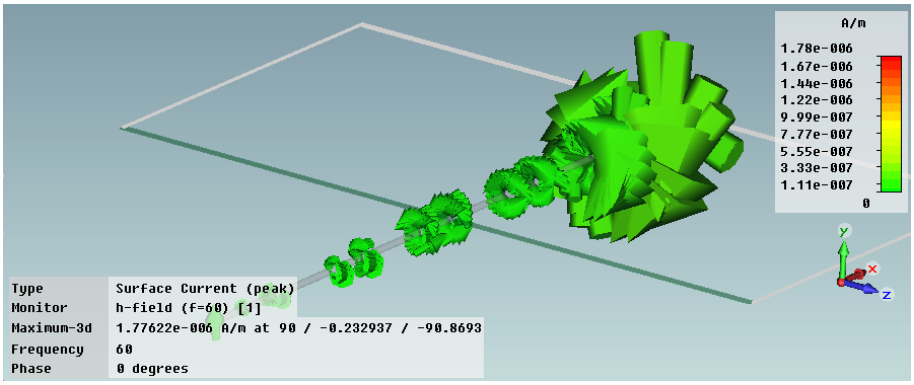

Figure 2.7 Induced current distribution for the 90° cross angle case

In general, the peak current is proportional to the induced area. When the CFT is perpendicular to the steel rebar, the induced area is smaller than that in the parallel case, hence smaller peak current was produced.

Assuming a zero cross angle, the vertical distance d is adjusted to investigate its impact on the induced current. When the vertical distance d is adjusted from 2.5 cm to 5.0 cm and 7.5 cm, the respective induced current distributions are obtained and shown in Figure 2.8 and Figure 2.9. It is observed from Figure 2.6, Figure 2.8 and Figure 2.9 that the peak current decreases from 4.31 nA for a vertical distance of 2.5 cm to 1.09 nA for a vertical distance of 7.5 cm. In other words, the peak current decreases with increasing vertical distance. Table 2.1 summarizes the peak induced current for cases with various cross angles and vertical distances.

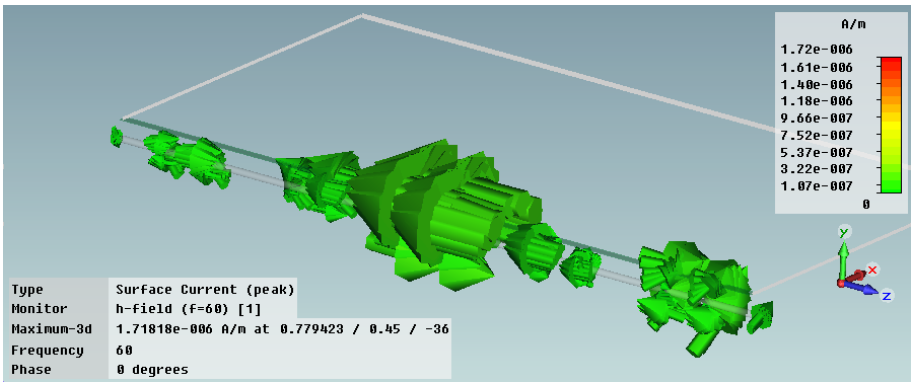

Figure 2.8 Induced current distribution for the case with d = 5 cm

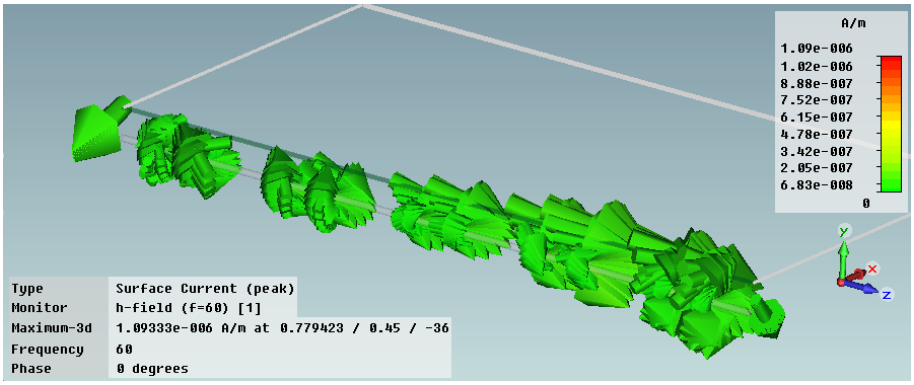

Figure 2.9 Induced current distribution for the case with d = 7.5 cm

Table 2.1 Maximum induced current with various cross angles and vertical distances

Cross angle (°)	Vertical distance (cm)	Peak induced current (nA)
0	2.5	4.31
	5.0	1.72
	7.5	1.09
90	2.5	1.78

A simulation model was also built for the steel rebar mesh used in the sidewalk construction as shown in Figure 2.9. In this model, the length and width of the CFT heating panel in the concrete slab is 1.8 m and 1.2 cm, respectively. The steel rebar is 1.8 m long and the diameter is 1.8 cm. Two steel rebars were modeled: one parallel to and 2.5 cm away from the CFT strips and the other perpendicular to and 4.5 cm away from the CFT heating panel. The CFT heating panel was powered by an AC source with 24 V and 60 Hz. The simulated results for the two steel rebars are shown in Figure 2.10 and Figure 2.11, respectively. It is seen that the peak current for the steel rebar perpendicular to the CFT is 4.25 nA and that for the steel rebar parallel to the CFT is 4.64 nA.

2.4 Summary

This chapter discusses the induced currents obtained from field measurement and computer simulations. Field measurement shows no measureable current in the steel rebar mesh. Computer simulations show that the expected induced current in the steel rebar mesh is about the level of nAs, which is well below the current resolution of the instrument used to measure the induced current in the field. In conclusion, this level of induced current is at the level of nA and we believe it is negligible as long as corrosion is concerned.

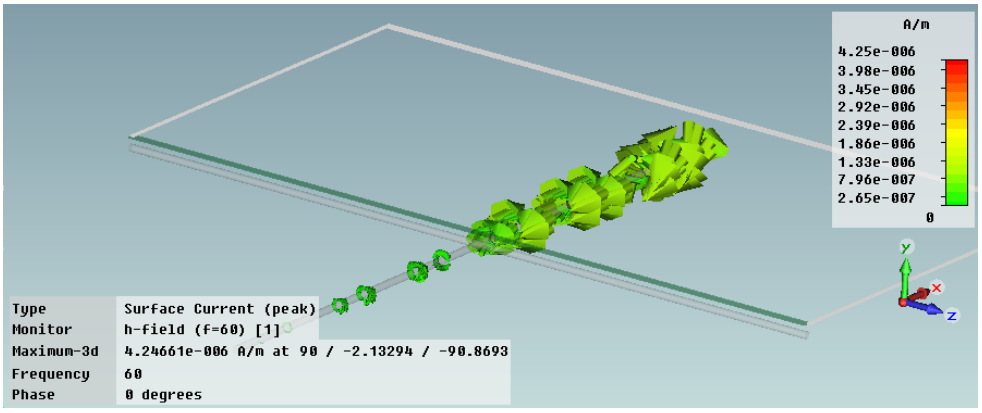

Figure 2.10 Induced current distribution in the steel rebar perpendicular to the CFT

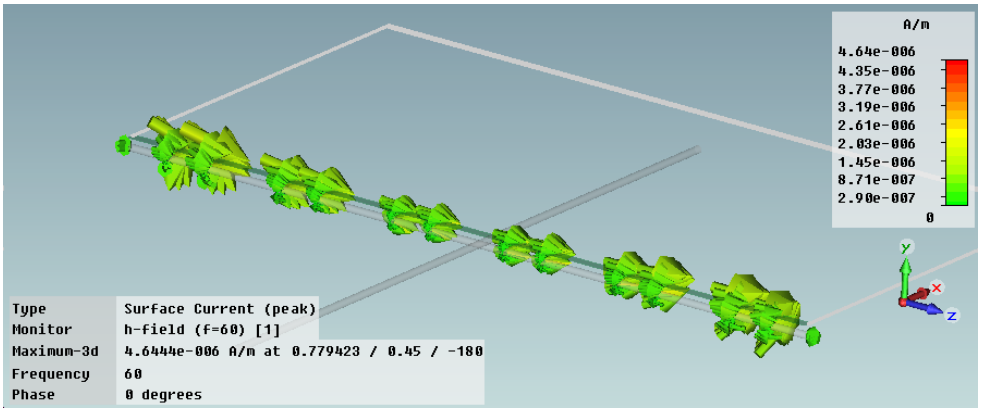

Figure 2.11 Induced current distribution in the steel rebar parallel to the CFT

CHAPTER 3: Automatic Control of CFT Heating Panel Deicing

3.1 Introduction

Yang et al. (2012) presented an innovative deicing technology and deicing experimental results. This technology uses custom-made CFT panels as the heating elements. A test sidewalk made of Portland cement concrete pavement embedded with such heating panels was constructed on the campus of University of Alaska Anchorage (UAA) for deicing experiments. In this facility, a power supply box and a data acquisition/control box were installed to house the power supply and data acquisition/control equipment, respectively. In the previous study, only manual On/Off control was available and it was envisioned that automatic controls would be able to significantly reduce the operating cost. This chapter presents the automatic controls developed and implemented at the experiment facility and their effects on the operating cost.

Error! Reference source not found. shows a block diagram of the automatic control system for the deicing experimental facility. The electrical power supply box consists of a power meter, three step-down transformers and three solid state relays. Power and energy usage can be tracked from the power meter. The transformers used in this deicing system are PH1000PG HPS Machine Tool Industrial Control Transformers with a primary voltage of 120/240V, a secondary voltage of 12/24 V, and a VA rating of 1000VA. During deicing experiments, the transformers are connected to 110V/60Hz AC power outlet and the heating panels are charged with a 24V AC for heat generation.

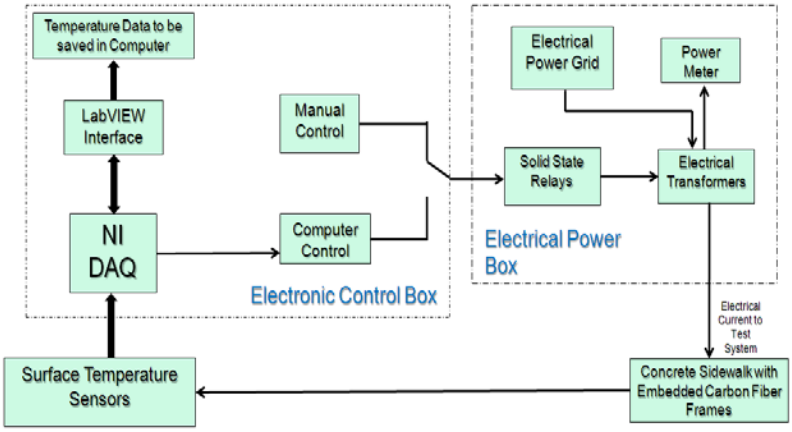

Figure 3.1 Block diagram of the automatic control system for deicing experiments

The electronic control box houses three units: an industrial computer, a data acquisition unit (NI 9188) and a power-switching unit. The NI-9188 is an Ethernet chassis manufactured by

National Instruments. It consists of a 16-channel thermocouple reader (NI 9213) and an 8-channel solid state relay driver (NI 9485). The data can be retrieved through a remote computer via the Internet. A LabVIEW-based interface was developed for data acquisition and temperature control (see Figure 3.2). The LabVIEW interface has the following capacities and their details will be discussed in the following sections: 1) web-based weather monitoring of the test site; 2) manual On/Off electrical heating of the CFT panels; 3) automatic ON-OFF control of sidewalk surface temperature; 4) Fuzzy Logic-based temperature control; and 5) data saving.

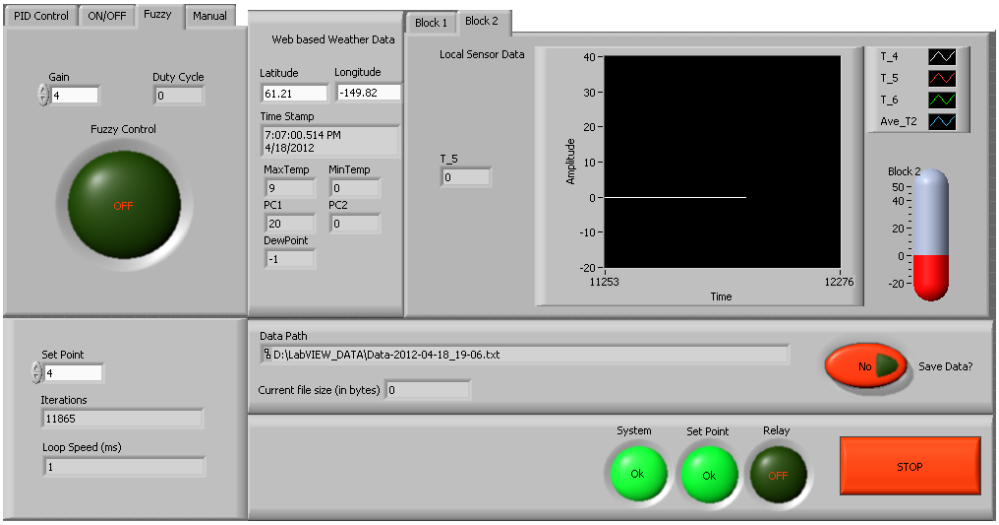

Figure 3.2 LabVIEW-based user interface for monitoring deicing experiments

3.2 Web-based weather monitoring

A web-based weather monitoring is included in the LabVIEW interface. This interface uses the Simple Object Access Protocol (SOAP) server. The SOAP server provides different sub virtue instruments (VI) which can be used to retrieve information about the location of interest and environmental data at that location. The different sub VIs offer choices to select the targeted area for deicing with area zip code, city and state name, and longitude and latitude information. Since the deicing technology may also be implemented at remote locations, longitude and latitude based sub-VIs are the preferred choice. The sub-VIs also offers flexibility of choosing different environmental parameters for weather monitoring. For this project, the SOAP was used to retrieve the weather information by using the longitude and latitude of the test site.

The weather forecast data is retrieved from the XML service of the National Digital Forecast Database (NDFD), which is a service providing the public, government agencies, and commercial enterprises with data from the digital forecast database of the National Weather Service (NWS). The NDFD database is updated every 45 minutes to 1 hour. The SOAP connects the LabVIEW interface to the NDFD database by request. Figure 3.3 illustrates the process of

retrieving weather data from the NWS. The following information is collected by the LabVIEW interface through SOAP request: Maximum and minimum temperatures, probability of precipitation and the dew point.

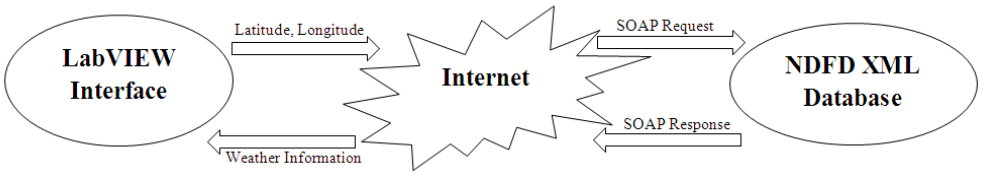

Figure 3.3 Retrieval of weather data via the LabVIEW interface

3.3 Description of Controllers

3.3.1 Manual On/off

The user interface is programmed to manually turn on or off the deicing system. A software manual switch is programmed to signal the solid state relay (SSR) through the NI data acquisition unit to turn on/off the electric current from the transformers to the CFT heating panels by an operator. Apart from a software manual switch, every block is connected to a 3-way switch to control the heating: one for turning the system off; the second for manual control of the heating; and the third for allowing the system to be controlled automatically via a user interface. The user interface has an ON/OFF controller and a Fuzzy Logic-based controller and the details are described in the following sections.

3.3.2 ON-OFF Controller

The heating of a concrete block to raise the surface temperature is a slow process. It takes a few hours to raise the temperature from sub-zero to above melting point at a limited input power. For this type of system, the ON-OFF controller generally shows optimized performance (Sen 2004). The ON-OFF controller is the simplest form of control and is often used in temperature controlled heating processes. When the temperature is less than the set-point temperature the heater is turned on at the maximum power; once the temperature is above the set-point, the heater is switched off completely. To keep the system temperature near the set-point temperature, the difference between the turn-on and turn-off temperatures are kept very small. This can be done in many ways by introducing a hysteresis or a dead zone in actuation. In this paper, a dead-zone is introduced to eliminate the temperature fluctuations. Figure 3.4 shows the block diagram of the ON-OFF controller.

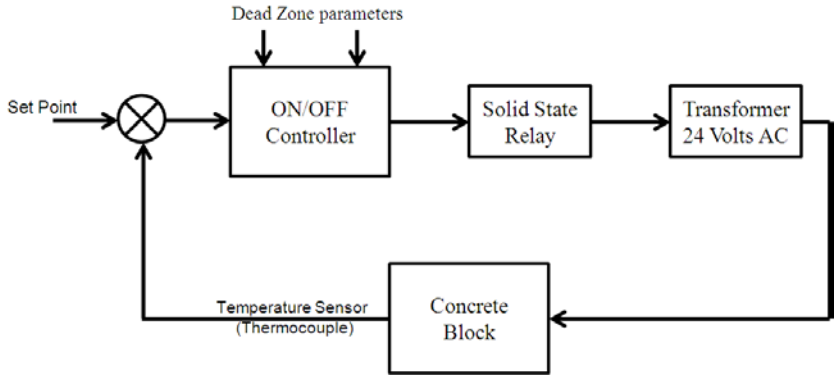

Figure 3.4 Block diagram of the ON-OFF controller

The ON-OFF controller described above can give optimal performance only under similar ambient conditions. However, environmental conditions are always changing and are sometimes very unpredictable. These fluctuating conditions affect its performance. To overcome this shortcoming, a Fuzzy Logic-based controller is developed to take into account environmental parameters and improve the system performance including operation cost.

3.3.3 Fuzzy Logic-based Temperature Controller

The Fuzzy Logic control approach attempts to mimic human control logic. Fuzzy refers to the fact that the logic involved can deal with concepts that cannot be expressed as "true" or "false" but rather as "partially true". The Fuzzy Logic has the advantage that the solution to the problem can be cast in terms that human operators can understand, so that their experience can be used in design of the controller. Fuzzy controllers are very robust, and can handle nonlinearities and model uncertainties of the system quite well. However, design of a Fuzzy Logic controller requires an in-depth knowledge of the system and its behavior.

Figure 3.5 presents a general block diagram of a Fuzzy Logic controller with four elements and these are the set of rules, interference mechanism, fuzzification and defuzzification. The set of rules contain the Fuzzy Logic quantification of expert knowledge of the system for high quality control. An inference mechanism describes the fuzzy outputs based on the expert's knowledge of system. Inference mechanism has two basic tasks: 1) determining the extent to which each rule is relevant to the current situation of the system and 2) drawing a decision based on the current input and information from the rule-base. In general, the inference mechanism works on the if/then principle and decides the output of the controller based on information from the sensor.

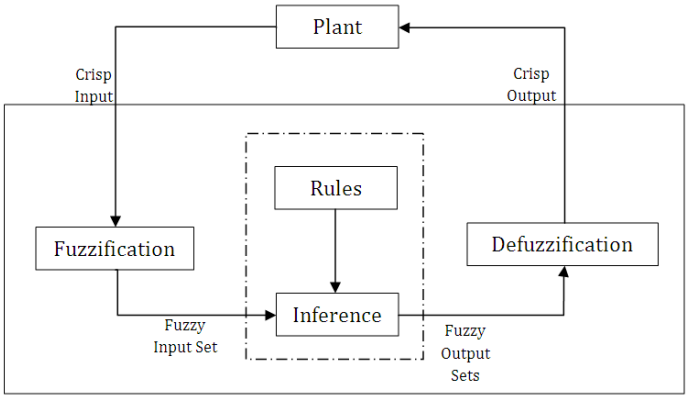

Figure 3.5 Block diagram of the Fuzzy Logic controller

In fuzzification, fuzzy sets are used to quantify the information in the rule-base. It can be defined as an interface which converts the controller crisp input into a fuzzy input set that can be understood by the inference mechanism, or “fuzzifies” the raw input of the sensor. Generally, a Singleton fuzzification function is used, which produces a fuzzy set that defines a membership function to quantify the information in the rule-base for the control output. Defuzzification is the interface used to convert decisions made by the inference mechanism to physical output for the controller to control the plant. There are different types of defuzzification strategies in existing Fuzzy Logic control systems. Some of these strategies include:

1. Center of gravity (COG): The crisp output is chosen by the center of area and area of each implied fuzzy set.

2. Center Average: The crisp output is chosen using the centers of each of the output and membership functions and the maximum certainty of each of the conclusions that represent the implied fuzzy set.

3. Maximum criterion: The crisp output is chosen as the maximum value that can be achieved for the overall fuzzy set.

4. Mean of maximum: The crisp output in this strategy is the mean value of all elements having maximum membership in their defined fuzzy set.

Generally, the center average defuzzification technique is used as it is easy to implement. A model of a fuzzy system can be expressed by using the product inference engine, Singleton fuzzifier, and center average defuzzifier, as

$$u_D(\mathbf{x}|\theta)=\frac{\sum_{l_1=1}^{m_1}\sum_{l_2=1}^{m_2}\bar{y}_u^{l_1 l_2}\left(\prod_{i=1}^{2}\mu_{A_i^{l_i}}(x_i)\right)}{\sum_{l_1=1}^{m_1}\sum_{l_2=1}^{m_2}\left(\prod_{i=1}^{2}\mu_{A_i^{l_i}}(x_i)\right)} \quad (1)$$

where the parameter matrix $\theta \in R^{\prod_{i=1}^{2} m_i}$ which consists of the adjustable parameter $\bar{y}_u^{l_1 l_2}$. Then the fuzzy controller can be rewritten as

$$u_D(\mathbf{x}|\theta)=\theta^T \xi(\mathbf{x}) \quad (2)$$

where $\xi(\mathbf{x})$ is defined as

$$\xi^{l_1 l_2}(\mathbf{x})=\frac{\prod_{i=1}^{2}\mu_{A_i^{l_i}}(x_i)}{\sum_{l_1=1}^{m_1}\sum_{l_2=1}^{m_2}\left(\prod_{i=1}^{2}\mu_{A_i^{l_i}}(x_i)\right)} \quad (3)$$

The fuzzy controller described above can be used to estimate the system nonlinearities and uncertainties by analyzing the crisp input with the fuzzy approach. For temperature control of the concrete test sidewalk, the input parameters for the Fuzzy Logic controller include surface temperature of concrete sidewalk block (T_L), environmental minimum temperature from the NWS website (T_W), dew point and probability of precipitation. The output parameter is the duty cycle for the PWM signal to activate the SSR. The duty cycle ranges from 0% to 100%. Figure 3.6 shows a block diagram of the Fuzzy Logic-based temperature controller for deicing application.

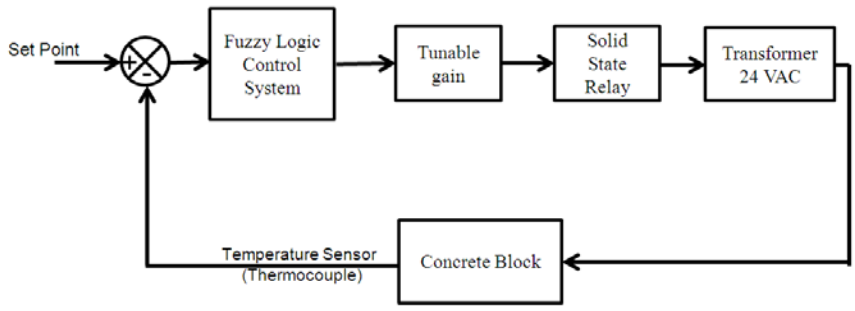

Figure 3.6 Block diagram of the Fuzzy Logic-based temperature controller

Generally, if the dew point is lower than the environmental temperature, probability of precipitation in the form of snow or rain is high in the area. For the Fuzzy Logic controller chances are moderate that rain or snow fall will occur if probability of precipitation is greater than 40%, and chances are considered to be very high if probability of precipitation exceeds 60%. The probability of precipitation under 40% is considered low for rain/snow fall. Table 3.1 and Table 3.2 list the fuzzy rules for the temperature controller. The temperature range for these rules is classified into five categories: Very Low (less than -15°C), Low (-10°~-5°C), Less Zero (-5°~-2°C), Zero (-2°~2°C), High (2°~5°C), and Very High (greater than 5°C).

Table 3.1 Fuzzy rules for probability of precipitation > 40% and dew point > min. temperature

T_W \ T_L	Very Low	Low	Less Zero	Zero	High	Very High
Very Low	Low/ Moderate	Low/ Moderate	High/ Moderate	High/ Moderate	Zero	Zero
Low	High/ Moderate	High	High	High	Zero	Zero
Less Zero	High	High	High	High	Zero	Zero
Zero	High	High	High	High	Zero	Zero
High	Moderate	Moderate	Moderate	Low	Zero	Zero
Very High	Moderate	Moderate	Low	Low	Zero	Zero

Table 3.2 Fuzzy rules for probability of precipitation > 60 and dew point > min. temperature

T_W \ T_L	Very Low	Low	Less Zero	Zero	High	Very High
Very Low	High	High	High/ Moderate	High/ Moderate	Zero	Zero
Low	High	High	High	High	Zero	Zero
Less Zero	High	High	High	High	Zero	Zero
Zero	High	High	Moderate	Moderate	Zero	Zero
High	Moderate	Moderate	Low	Low	Zero	Zero
Very High	Moderate	Moderate	Low	Low	Zero	Zero

3.4 Experimental Results

These automatic controllers were tested under natural conditions at the deicing experimental facility on the UAA campus. In the manual control, a typical operation is to turn on the heating system to melt the snow or ice observed on the sidewalk through a webcam, and turn it off once the sidewalk surface is clear of snow or ice. The surface temperature can reach up to 12°C during a 20-hour-long experiment. Details on temperature variation with time can be found in Yang et al. (2012).

Figure 3.7 shows the variation of temperature with time obtained from one of many experiments with the ON/OFF controller. In this experiment, the concrete test sidewalk did not cool down to below the freezing point under natural conditions after a previous deicing experiment before it was switched to the ON/OFF controller. This explains why the surface temperature in Figure 3.7 starts from above 0°C. The set-point temperature was 4°C. It is seen from Figure 3.7 that the controller was able to keep the surface temperature between 0° and 4°C, just as expected. From this plot one can observe a few temperature spikes in the range of 5° to 10°C, the cause of which will be discussed later.

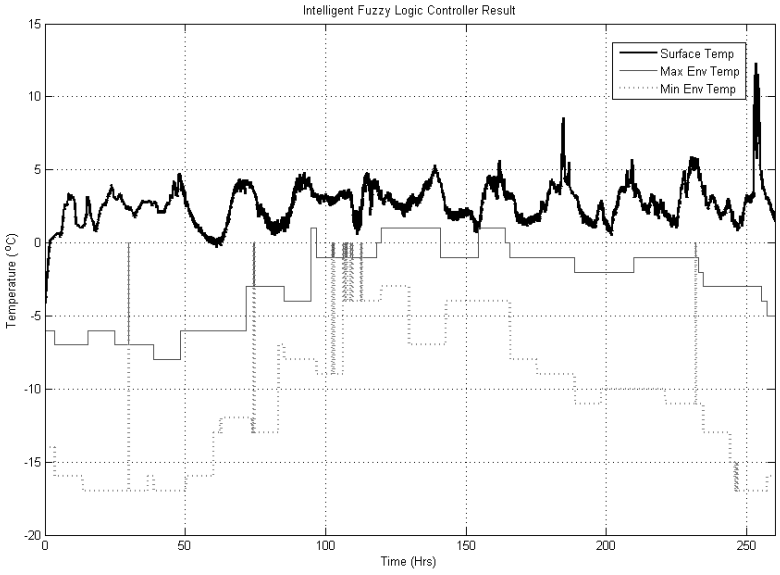

Figure 3.7 Temperature variation with time for the ON/OFF controller

Figure 3.8 presents the variation of temperature with time over a short period of time (12 hours) for the Fuzzy Logic-based controller. The target surface temperature was set to be around 4°C. It can be seen that it took the controller about 4 hours to raise the surface temperature from -2.5° to above 0°C. It is also observed that the controller was able to maintain the surface temperature between 0° and 4°C.

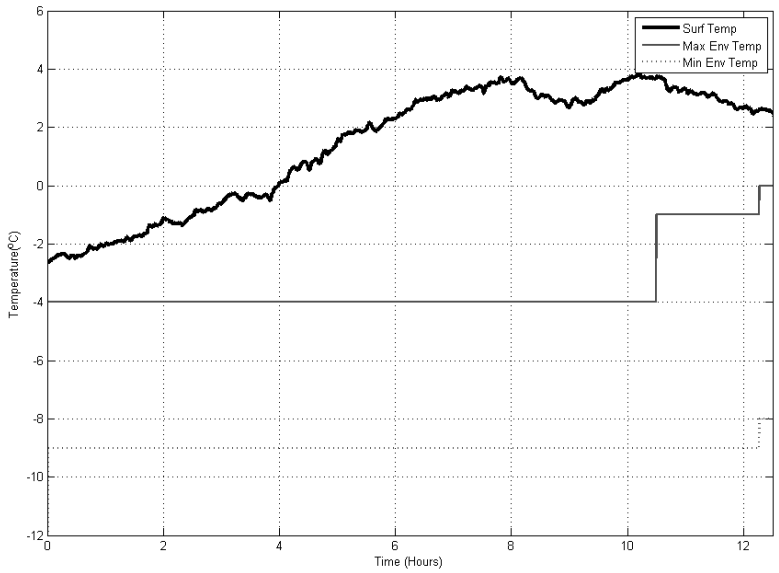

Figure 3.8 Temperature variation over 12 hours for the Fuzzy Logic-based controller

Figure 3.9 presents the variation of temperature over a longer period of time (approximately 260 hours) for the Fuzzy Logic-based controller. The target surface temperature was chosen to be around 4°C. It can be seen that the Fuzzy Logic-based controller was able to keep the temperature between the freezing point and the target surface temperature under different environmental conditions. A few peaks in the range of 5° to 12.5°C can again be observed in this figure.

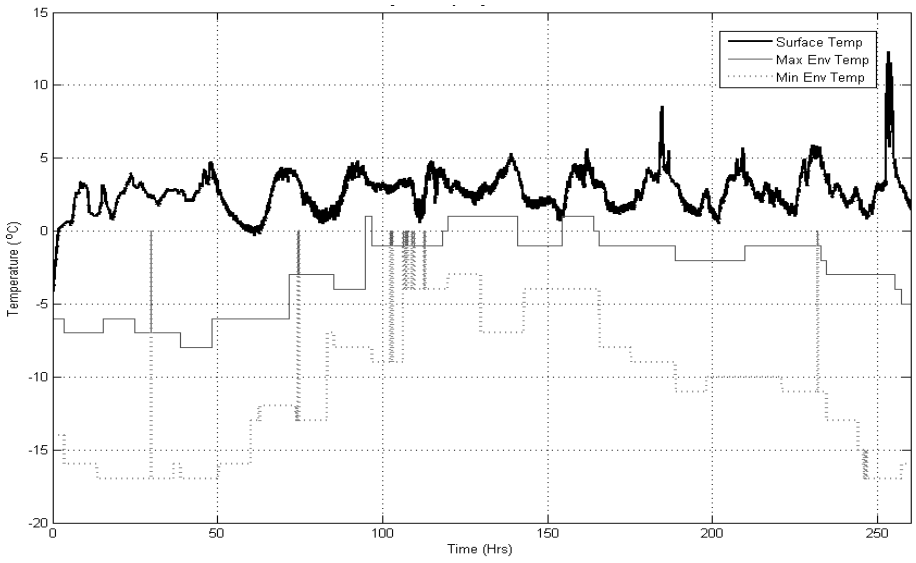

Figure 3.9 Temperature variation over 260 hours for the Fuzzy Logic-based controller

The high peaks in the range of 5° to 12.5°C can be seen in the surface temperatures from both controllers. This can be attributed to the sunlight and other environmental effects. During the day time, the sunlight directly falling on the sidewalk concrete blocks helps raise the surface temperature. Since the thermocouple used to measure the surface temperature is exposed to sunlight as well, it may also give higher temperature reading during day time.

3.5 Power Consumption Analysis

Cost effectiveness for both installation and operation is a very important factor that affects whether a new deicing system should be adopted for application. For electrical deicing systems, potential users are particularly sensitive to the recurring operating cost. In an earlier study, Yang et al. 2012 compared the installation cost with other existing technologies and found that the CFT-based deicing system has relatively low installation cost and much lower operating cost. It was envisioned that this system could be made more efficient if an automatic control scheme is developed and implemented to prevent waste of electrical power when there is no ice or low probability of precipitation.

Table 3.3 and Table 3.4 present the power consumption data for deicing experiments with the ON/OFF and Fuzzy Logic-based controllers, respectively. The experiments were conducted from Mar. 2 to Mar. 19, 2012. Assuming the electricity cost at \$0.2/kWh, the average cost for the ON/OFF controller was \$0.245/[day.m^2], and that for the Fuzzy Logic-based controller was \$0.178/[day.m^2]. The average cost for the manual control based on the deicing experiment data reported in (Yang et al. 2012) was \$0.61/[day.m^2].

Table 3.3 Power consumption of the deicing experiments with the ON/OFF controller

Date	Time b/w reading (hrs)	Energy Usage (kWh)	Energy Cost (\$)	Energy Cost (\$/day)	Cost/Unit Area (\$/[day.m^2])
03/02~05/2012	80	22.157	4.4314	1.3294	0.298
03/05~06/2012	22	4.03	0.8060	0.8784	0.197
03/06~07/2012	20	3.81	0.7620	0.9144	0.205
03/07~09/2012	48.33	8.786	1.7572	0.8736	0.196
Total	170.33	38.7830	7.7566	1.0929*	0.245*

Table 3.4 Power consumption of the deicing experiments with the Fuzzy Logic-based controller

Date	Time b/w reading (hrs)	Energy Usage (kWh)	Energy Cost ($)	Energy Cost ($/day)	Cost/Unit Area ($/[day.m^2)
03/09~12/2012	76.5	15.197	3.0394	0.9535	0.208
03/12~13/2012	23.5	4.545	0.9090	0.9283	0.151
03/13~14/2012	22.33	3.142	0.6284	0.6753	0.156
03/14~19/2012	123	17.79	3.5580	0.6942	0.166
Total	245.33	40.6740	8.1348	0.7968*	0.178*

Table 3.5 Comparison of energy consumption and cost for the three control methods

Controller Type	Energy Consumption ([kWh/day.m^2])	Unit Energy Cost* ($/[day.m^2])
Manual Control	3.05[a]	0.61[a]
On-Off Controller	1.25	0.25
Fuzzy Logic Controller	0.90	0.18

Note: Cost for sidewalk preparation and system components is not considered.
* electricity cost assumed to be $0.2/kWh
a values calculated from an earlier study (Yang et al. 2012).

Table 3.5 presents a comparison of the energy consumption and cost for the three control approaches. From Table 3.5, it can be stated that the deicing system with the ON/OFF controller or the Fuzzy Logic-based controller demonstrates excellent efficiency in terms of power consumption. Compared with the manual control, the ON/OFF controller reduces the power consumption or cost of the deicing system by 59%, and the Fuzzy Logic-based controller reduces that by 70%. In addition, the Fuzzy Logic-based controller reduces the power consumption by 28% when compared with the ON/OFF controller.

3.6 Summary

In this chapter, the design and development of two automatic temperature controllers for resistive heating-based deicing technologies are presented. The controllers–an ON/OFF

controller with a dead-zone and an advanced Fuzzy Logic-based controller–are implemented at the deicing experimental facility with the CFT-based deicing system. A LabVIEW interface was built to enable the remote access and monitoring of the deicing experiments. A series of deicing experiments were carried out in the Spring of 2012. It was found that the performances of these controllers in all the deicing experiments were satisfactory and these controllers consumed much less power than the manual On/Off control previously tested. Compared with the manual control, the ON/OFF controller and advanced Fuzzy Logic-based controller reduce the power consumption or cost by 59% and 70%, respectively. In addition, the Fuzzy Logic-based controller is 28% more efficient than the ON/OFF controller. The design and implementation of the Fuzzy Logic-based controller for deicing application represents a major technical contribution of this paper. It is envisioned that after improving the controller model for effects of environmental changes, such as daily temperature cycles and wind conditions, the Fuzzy Logic-based controller can be more efficient. With certain adaptions this advanced controller is also applicable for other resistive heating-based deicing technologies.

CHAPTER 4: Structural Integrity of Concrete Slab with Embedded CFT Heating Panel

4.1 Introduction

As discussed in Chapter 1, one of the important issues that needs to be addressed is whether the embedment of the CFT will affect the structural integrity of the concrete slab. The pullout test of the CFT embedded in concrete slabs was conducted to study the bonding or lack of bonding between the concrete and the CFT with or without coating. Both three- and four-point bending tests of concrete slabs were performed to investigate how the embedded CFT will affect the flexural behavior of the concrete slab. Slabs embedded with steel rebars have also been tested for comparison. This chapter presents CFT material characteristics, test specimen configuration, test setup and data acquisition system, and results and discussions for both the pullout and bending tests. The test results also help to answer whether the CFT can survive cracking of concrete slabs.

4.2 CFT Material Characteristics

Cytec Thornel® T-300 3K carbon fiber tape was used for all tests. Table 4.1 presents the basic properties of the CFT. Note that the given tensile strength is for individual carbon fibers. Due to the arrangement of fibers in the CFT, such high tensile strength may not apply to the CFT.

Table 4.1 the CFT properties

Property	Value
Number of filaments per strand	3000
Number of strands of the CFT	30
Filament diameter	7 μm
Density	1.76 g/cm^3
Tensile strength (ultimate)	3,650 MPa
Elongation at Break	1.4%
Modulus of Elasticity	231 GPa

To characterize the CFT material, several tensile tests were conducted with the INSTRON 4482 testing machine (see Figure 4.1). To understand the tensile behavior of the CFT under various loading conditions, the following 3 parameters were varied during test:

- Strain/displacement rate,
- Length of CFT specimen, and
- Coating (with or without epoxy).

Figure 4.1 (a) and (b) show the test setup and a snapshot of the CFT during the tensile test. Figure 4.2 presents the test result. The strain rate was varied by altering the displacement rate of the testing machine while using the same length of the CFT (3 in. long). As shown in Figure 4.2, the strain rate has limited effect on the peak tensile force and the overall tensile behavior of the CFT. The CFT did not fail suddenly. In the post-peak part of the curves, after the first failure/breaking of several carbon fibers, there is a slight delay in failure of the remaining carbon fibers in the CFT (see Figure 4.1and Figure 4.2).

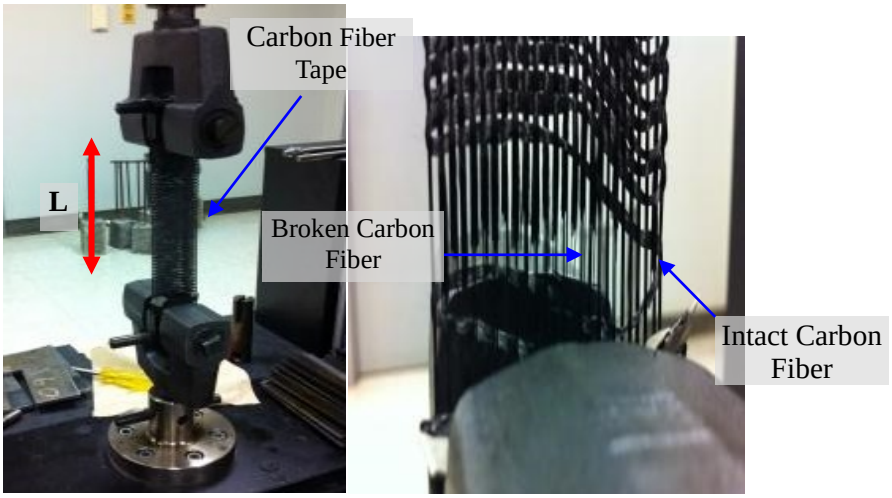

(a) (b)

Figure 4.1 Tensile test of the CFT: (a) Test setup, and (b) snapshot of the CFT during tensile test.

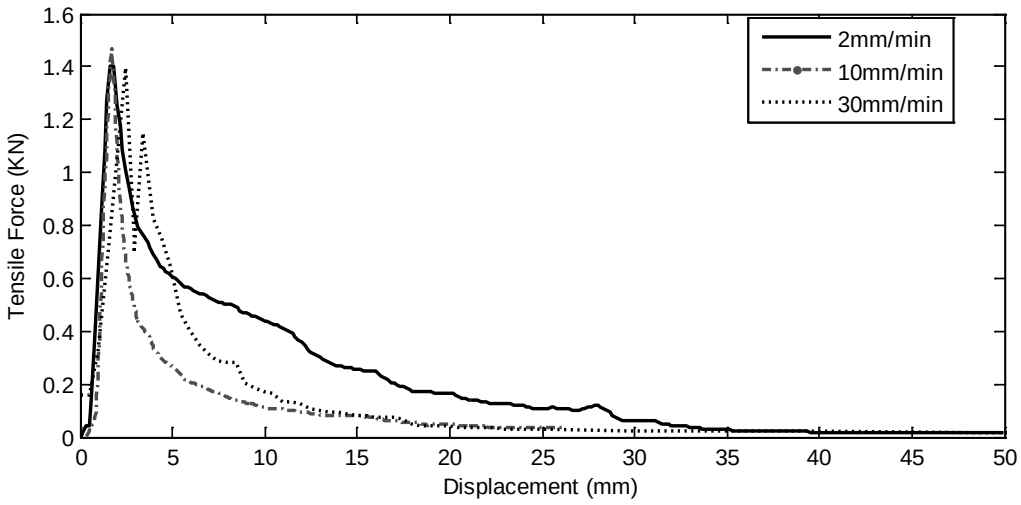

Figure 4.2 Effect of strain rate on the tensile behavior of the CFT

Another experiment was conducted to determine the effect of the CFT length on its tensile behavior. Note that the length L refers to the net distance between the two clamps (see Figure 4.1a). Test results in terms of tensile force vs. displacement for three CFTs with its length varying from 3 in. to 8.5 in. were shown in Figure 4.3. It is clear from this figure that the length adversely affects the tensile strength of the CFT. It was found that during the test, due to lack of proper clamping not all fibers in the CFT were loaded at the same time.

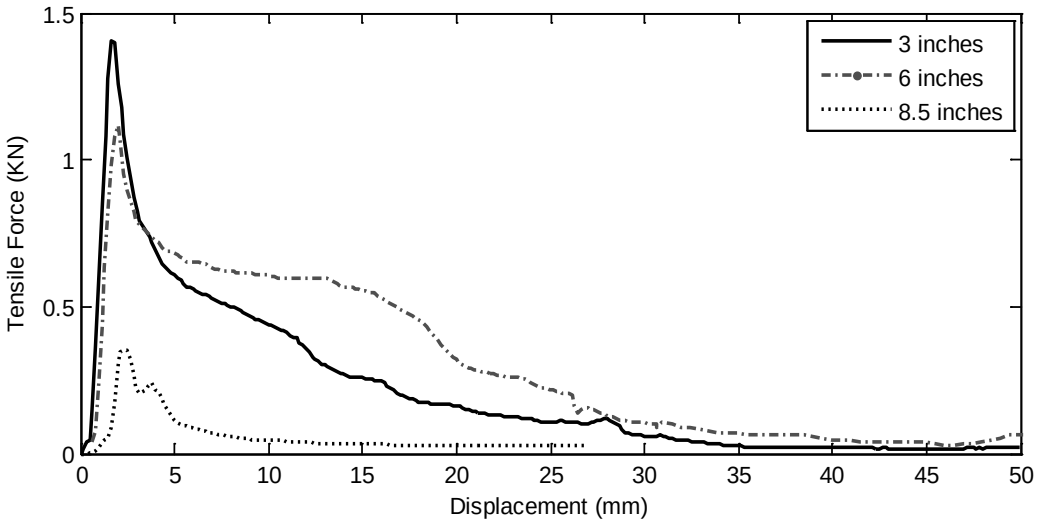

Figure 4.3 Tensile behavior of the CFT with increasing length

The CFT heating panel used for deicing was coated with thermally conductive electrically insulating silicone rubber epoxy. One experiment was performed to investigate the effect of such coating on the tensile behavior of the CFT. The epoxy used for test was similar to the epoxy (50-1225R Silicone Rubber, Epoxies.com) used in coating the CFT heating panel embedded in the test sidewalk at University of Anchorage Alaska. Specimens used for the tensile test were 3 in. long and the displacement rate applied was 30 mm/min. Figure 4.4 presents the tensile force vs. displacement for the coated CFT; that for the bare CFT is also shown for comparison. It can be observed that the presence of the silicon rubber coating on the CFT prevented it from developing high tensile force. The main reason for this is the slippage between the CFT and the clamp, causing uneven loading of fibers in the CFT (see Figure 4.5). Uneven loading applies a relative high tensile force on a small portion of the fibers, while the rest fibers with coating slipped through the grips. Due to friction between the epoxy and the CFT, a constant tensile force value was recorded during the slipping stage. A force plateau for the CFT coated with silicone rubber epoxy can also be seen in Figure 4.4. In summary, the bare or uncoated CFT can provide higher strength, while the silicone rubber epoxy coated CFT can provide the desired ductility, or allow the slippage between the gripper and the CFT. This behavior may prove to be beneficial since it

can increase the survivability of the CFT heating panel embedded in concrete slabs during concrete cracking.

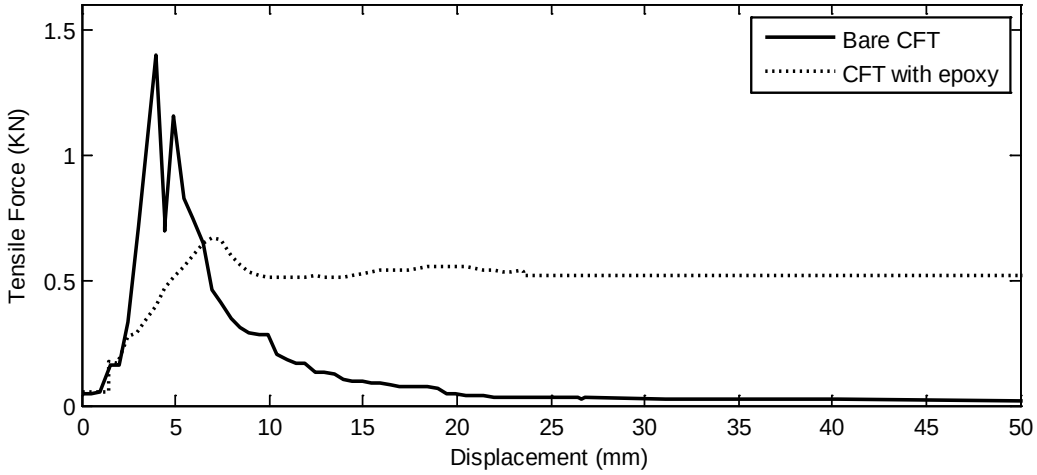

Figure 4.4 Tensile behavior of the CFT with or without silicone rubber epoxy coating

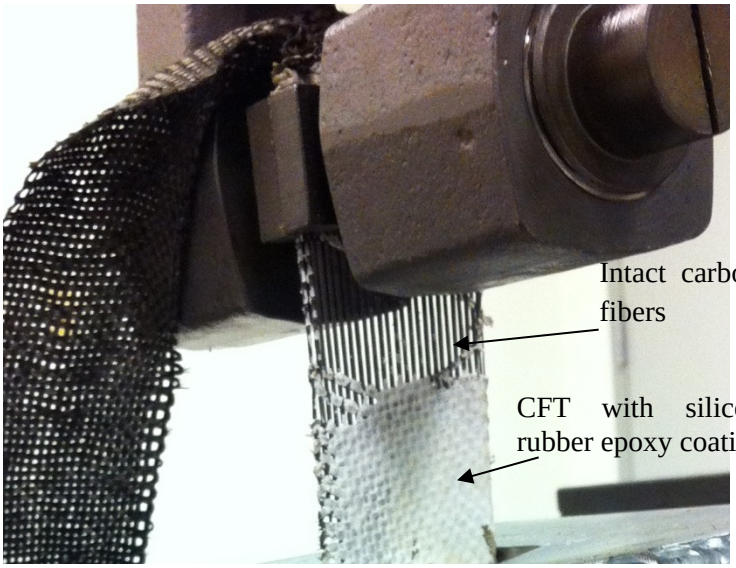

Figure 4.5 Damaged CFT coated with silicone rubber epoxy during tensile test

Slippage is observed between the grips and the bare CFT or silicone rubber epoxy coated-CFT. To investigate whether the slippage and regular (rigid) epoxy coating would affect the tensile behavior of the CFT, tensile tests were performed on two specimens: one bare or uncoated CFT and the other fully coated with high-strength rigid epoxy A-1101 (www.Fibreglast.com). The ends of both specimens – bare and rigid epoxy-coated CFT – were heavily coated with A-1101 to create a gripping area for improving alignment of fibers during loading. The strain rate

was 30 mm/min and specimens were 3 in. long. Figure 4.6 a and b show two snapshots of the tested CFT specimens with or without coating, respectively. Figure 4.7 presents the tensile force vs. displacement for both coated and uncoated CFT. Comparing Figure 4.7 with the tensile behavior for “Bare CFT” in Figure 4.4, it is clear that the peak tensile force of the CFT increases from 1.4 kN when the grip directly acts on the CFT to 5.0 kN when the grip acts on the CFT coated with rigid epoxy. This shows that, with proper clamping, the CFT can develop much higher tensile force.

Tensile strength of A-1101 epoxy is 49.6 MPa, and that for the carbon fiber is 3650 MPa. It is safe to assume that a coating with A-1101 will not affect the actual strength of the CFT. This is also evidenced by the results presented in Figure 4.7. No appreciable difference in the peak tensile force can be observed from Figure 4.7 for “Bare CFT” and “CFT with Epoxy (Hard)”. It is clear, however, that the coating of rigid epoxy alters the failure mode. The bare CFT reaches a peak tensile force, and drop sharply, but does not completely break. The CFT with rigid epoxy reaches a peak tensile force at a larger displacement relative to the bare CFT case, and sustains a high tensile force at the CFT elongated and suddenly breaks.

These characterization tests showed that the peak tensile force developed in the CFT is sensitive to strain or displacement rate, length of the specimen, and the clamping. Flexible coating such as silicone rubber epoxy allows slippage between the gripper and the CFT, and rigid coating can improve clamping, allowing the CFT to develop much higher tensile force.

(a) A-1101 coated CFT specimen

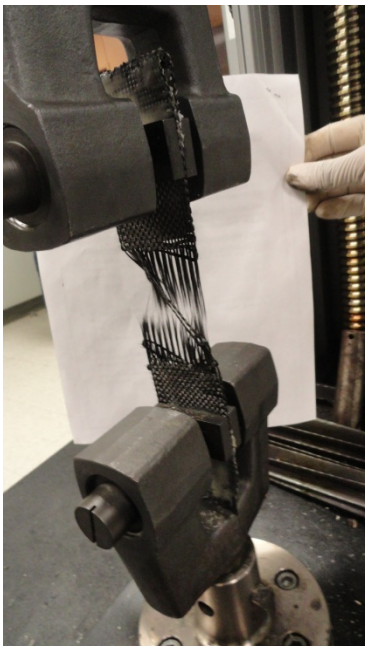

(b) Pure CFT specimen with ends coated by A-1101

Figure 4.6 CFT test specimens after tensile testing

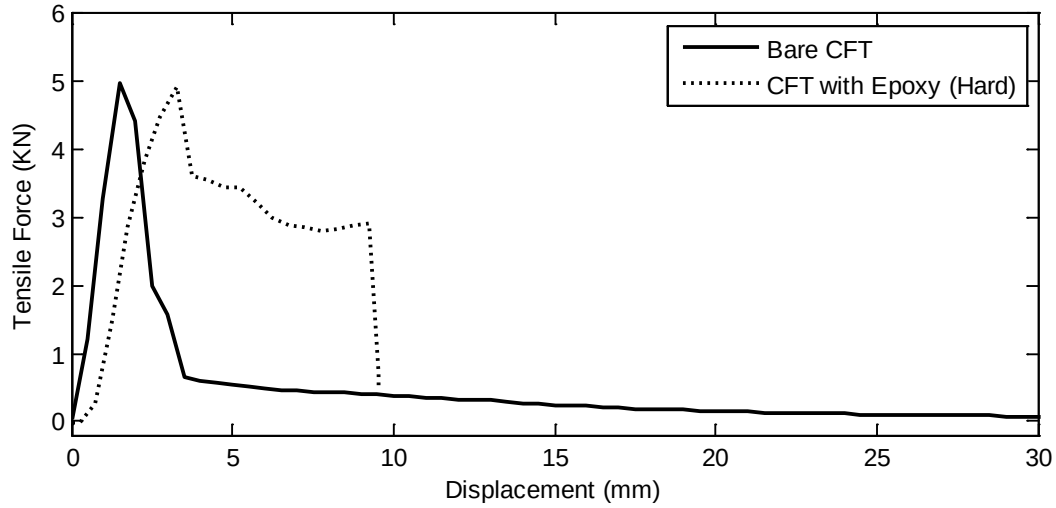

Figure 4.7 Tensile behavior of the CFT with its end coated by rigid epoxy coating

4.3 CFT Pullout Test

4.3.1 Specimens for the Pullout Test

The bonding between the CFT and concrete is important since it not only affects the flexural behavior of the concrete slab with embedded CFT, but also impacts the survivability of the CFT heating panel during cracking of concrete slab. The pullout test was conducted to study the bonding between the CFT (uncoated or coated) and concrete, and provide information for addressing the question of how large a crack the CFT heating panel can survive and still function as heating element for deicing. Pure CFT and CFT coated with silicone rubber epoxy (50-1225R Silicone Rubber, Epoxies.com) were considered. Specimens with embedded steel rebars were prepared and tested for comparison. Figure 4.8 shows the general dimension and types (steel rebar or CFT) of the pullout test specimens. Contact surface area per unit length of embedded elements in the concrete block was maintained constant at 4 sqare in. per in. embedment.

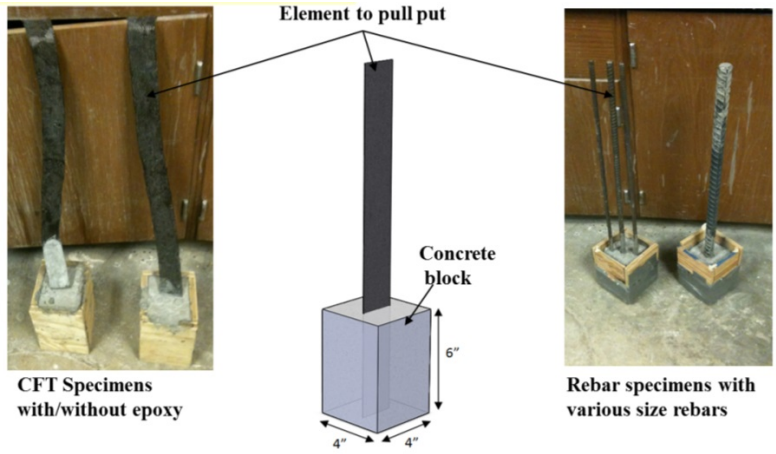

Figure 4.8 Specimens for the pullout test

Mix proportions for the concrete are listed in Table 4.2. All specimens were allowed to wet cure for 28 days. Standard compression test performed on concrete cylinders of 6 in. diameter showed an average concrete strength of 6.75 ksi. Figure 4.9 shows a specimen after the compression test.

Table 4.2 Concrete mix proportion

Content	Weight (lbs)
Cement	18
Sand	24
Aggregate	40
Water	7

Figure 4.9 Concrete specimen after compression test

4.3.2 Test Setup and Data Acquisition

A tension/compression testing machine (INSTRON 4482) was used to perform the pullout test. A safety cage (see Figure 4.10) was fabricated to hold the specimen stationary and enclose it at the same time, as sudden failure/breaking of concrete might send concrete pieces flying around. It was observed that the safety cage successfully entrapped the debris during tests. Data acquisition was performed using NI LabVIEW-based data acquisition system dedicated to the INSTRON 4482 testing apparatus.

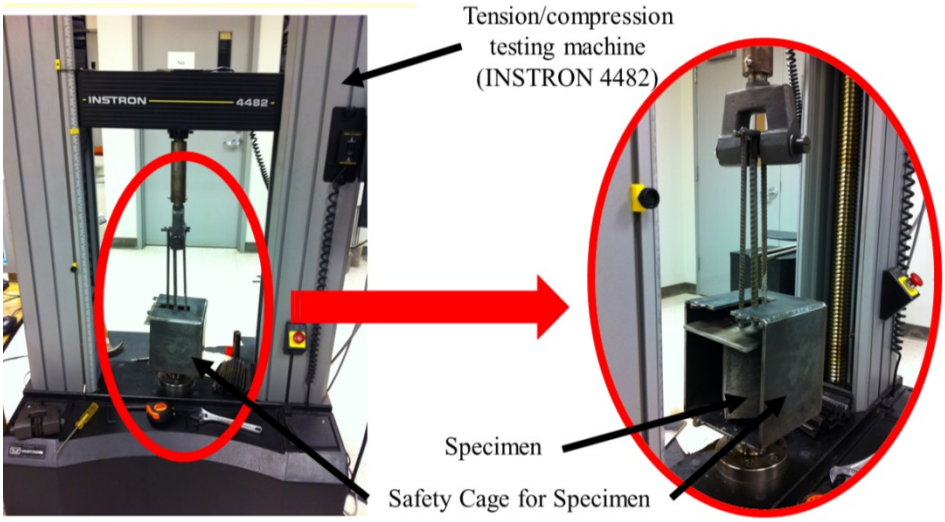

Figure 4.10 Test setup for the pullout test

4.3.3 Results from the Pullout Tests

Figure 4.11 shows the results of the pullout test performed on the concrete specimen with steel rebars. The sudden drop in tensile force observed in Figure 4.11 indicates the sudden debonding or slipping of steel rebar due to cracking. Figure 4.12 shows the broken concrete specimen inside the safety cage.

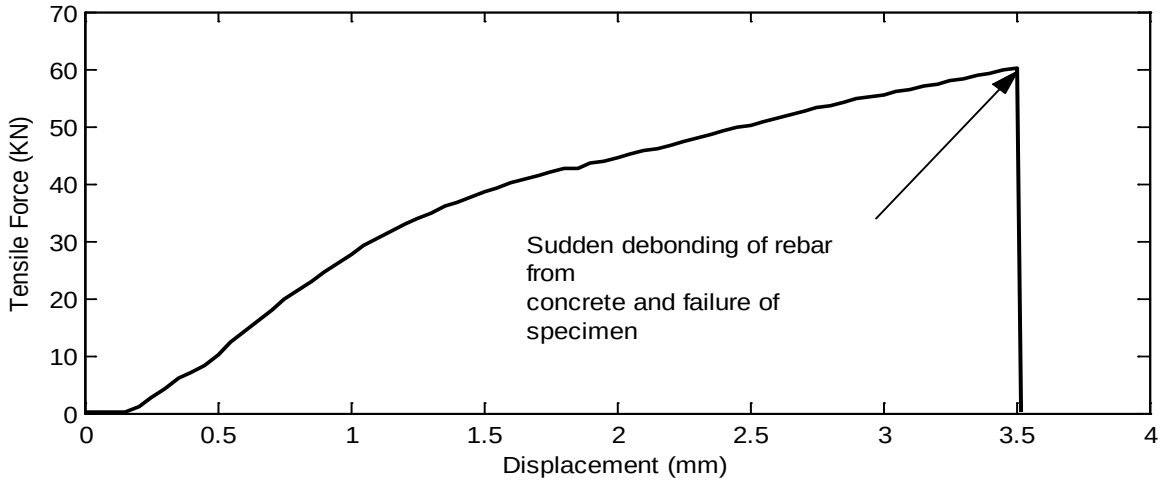

Figure 4.11 The response of specimen with steel rebars in the pullout test

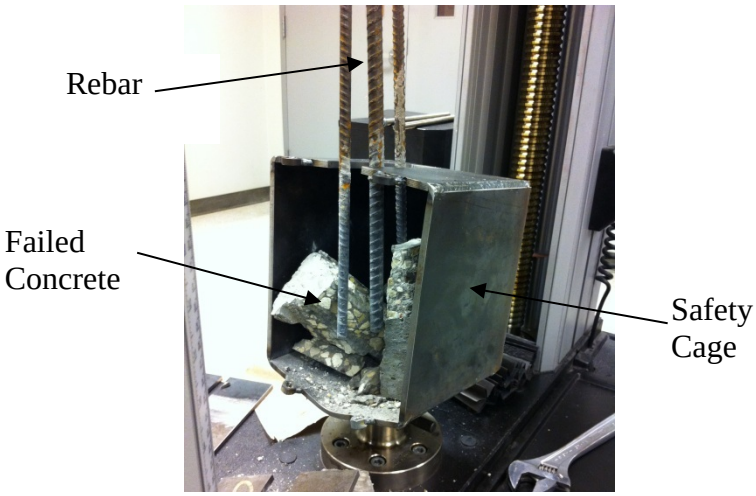

Figure 4.12 Concrete specimen with steel rebar after the pullout test

The CFTs with or without silicone rubber epoxy coating embedded in the concrete specimens were tested. In the actual application, epoxy helps to electrically isolate the CFT from concrete for safety concerns. Distance between the top clamp and top surface of concrete block was 2 in., and the displacement rate to pull the CFT was maintained at 30 mm/min. Figure 4.13a and b show that the CFT failed or broke outside the concrete specimen during the pullout test. This behavior indicates that the strength of the bonding between concrete and CFT with or without silicone rubber epoxy coating exceeds that of the CFT itself.

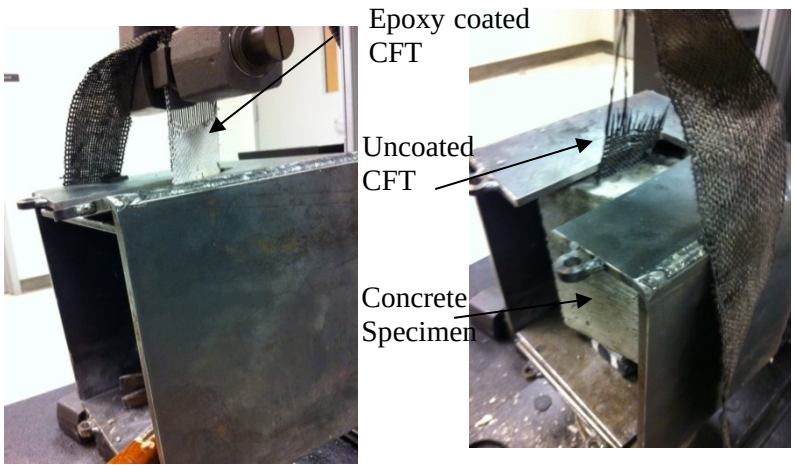

(a) With epoxy coating (b) Without epoxy coating

Figure 4.13 Snapshots of the CFT after the pullout test

4.4 Three- and Four-point Bending Tests

4.4.1 Test Parameters and Specimen Configuration

In order to understand the effect of CFT on the flexural behavior of concrete slabs and investigate the survivability of the CFT as heating elements during concrete cracking, two types of bending test – three- and four-point bending tests – were conducted. Three-point bending test of small-scale specimens is easier to conduct. However, both bending and shear are applied to the specimen. To simulate the pure bending of a large concrete slab induced by vehicle loading, four-point bending tests were also performed.

Figure 4.14a illustrates an 18 in. long, 8 in. wide, and 4 in. thick concrete specimen embedded with two 2 in. wide and 20 in. long CFT embedded at 1 in. from bottom. Figure 4.14b illustrates the concrete specimen with the same dimensions embedded with two 3/16 in. diameter steel rebars for comparison. Steel rebars were placed at the same location as the CFT. Note that no anchors were used for the CFT. Two specimens of each type were casted for 3-point bending test.

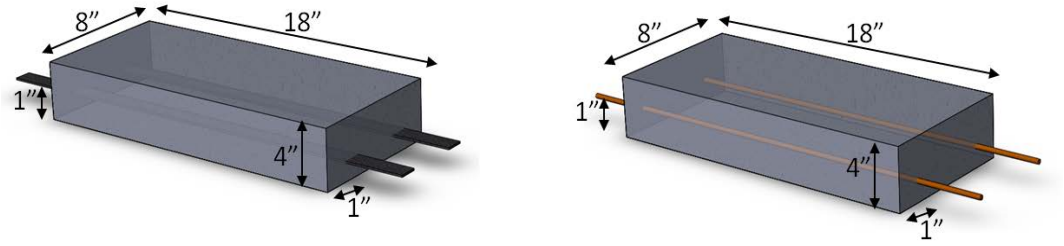

(a) Specimen with CFTs (b) Specimen with steel rebars

Figure 4.14 Schematics of three-point bending test specimens

Four-point bending test was performed on large-scale specimens of 60 in. long, 12 in. wide and 4 in. thick (see Figure 4.15). Similar to three-point bending test, one specimen with three bare CFTs and one specimen with 3/16 in. steel rebar were prepared for comparative study, as shown in Figure 4.16.

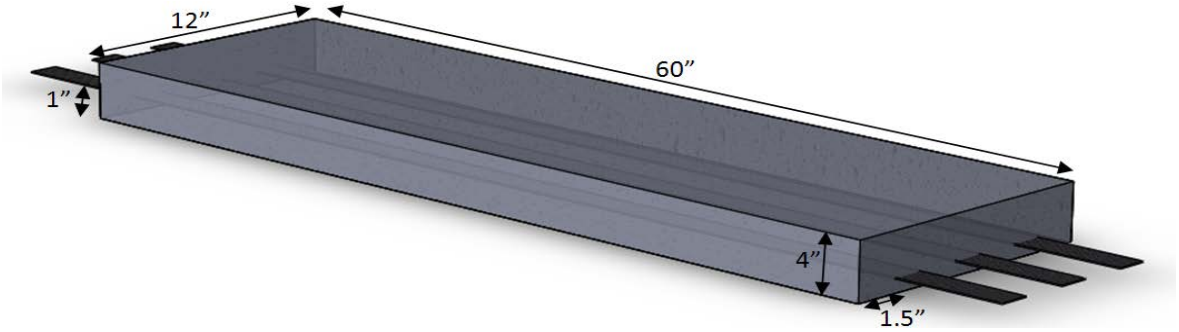

Figure 4.15 Schematics of large-scale specimens

Figure 4.16 Large-scale specimens with the CFTs and steel rebars

Four-probe electrical resistance monitoring was used to monitor the integrity of the CFT during the four-point bending test. Figure 4.17 shows that the ends of the CFT were connected to create a series connection of CFT for 4-point resistance monitoring. Electrically conductive tape was used to improve the contact between probes and the CFT. Increases in the electrical resistance values during test would indicate the internal breaking of carbon fibers.

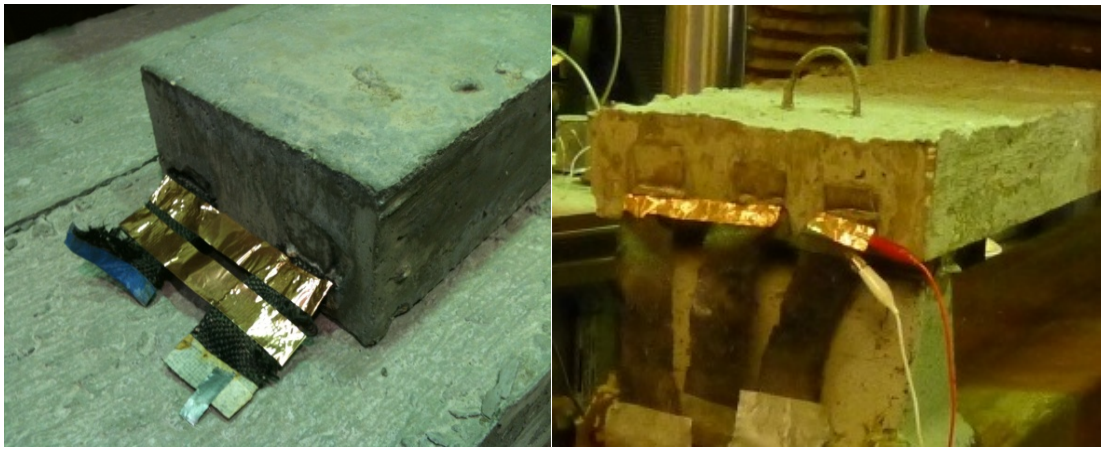

(a) Small-scale specimen (b) Large-scale specimen

Figure 4.17 Four-probe resistance monitoring connections

4.4.2 Test Setup and Data Acquisition

The setup for three-/four-point bending test consists of the following three units:

- Tension/compression testing machine
- Deflection monitoring system, and
- Resistance (integrity) monitoring system.

Testing equipment includes a tension/compression machine, a laser sensor, a source meter and data acquisition systems. The arrangement of these systems is illustrated in Figure 4.18.

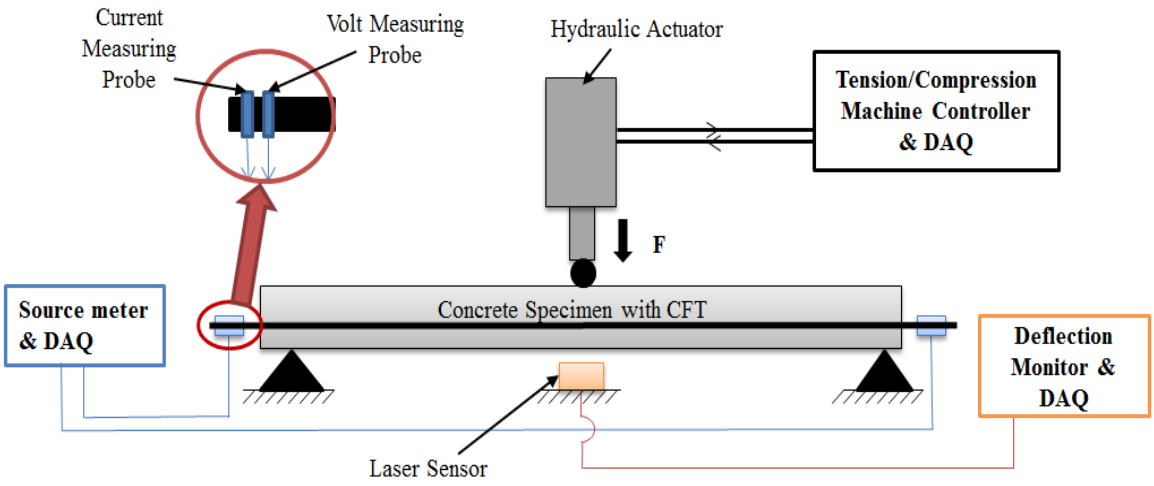

Figure 4.18 Schematics of the test setup

A Tinius Olsen type "A" testing machine was used for the bending test (see Figure 4.19). This hydraulic tension/compression testing machine can generate up to 60,000 lbfs with resolution of 10 lbfs and has a dedicated data acquisition system.

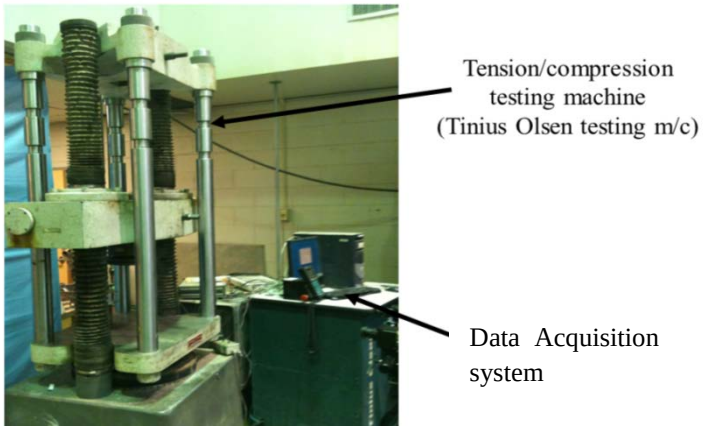

Figure 4.19. Tinius Olsen testing machine

A test procedure as illustrated in Figure 4.20 was developed for the safety of the operator and the device during tests. According to this procedure, if the value of the force reaches 60% of the maximum force achieved in the last 15 sec., the device halts itself. This sudden drop in force can only occur either due to sudden failure/cracking of concrete or malfunction of the device.

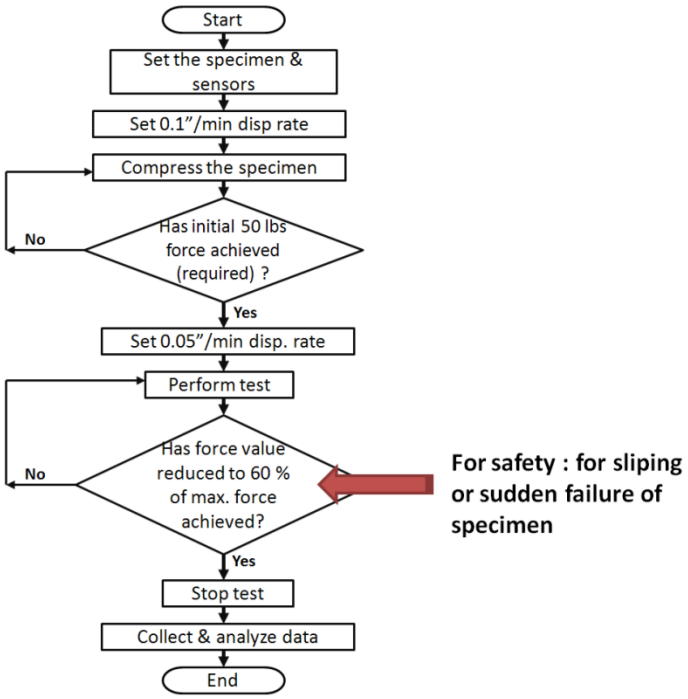

Figure 4.20 Procedure for the bending test

Two laser sensors (Keyance LB-11) were used to monitor the deflection of the specimen. As shown in Figure 4.18 and Figure 4.21, sensors were placed below the mid span of concrete specimen. A dSPACE system was used for acquisition of data from laser sensors.

Figure 4.21 Deflection monitoring by laser sensors

Figure 4.22 shows the resistance or integrity monitoring system by using four-point probe resistance measurement and a source meter. All CFTs were connected in series as the complete failure of a single CFT in parallel can be misunderstood as partial failure of all CFTs. With series

connection, complete failure (breaking) of any CFT during the test can be identified easily as the failure will change the resistance to a very high value.

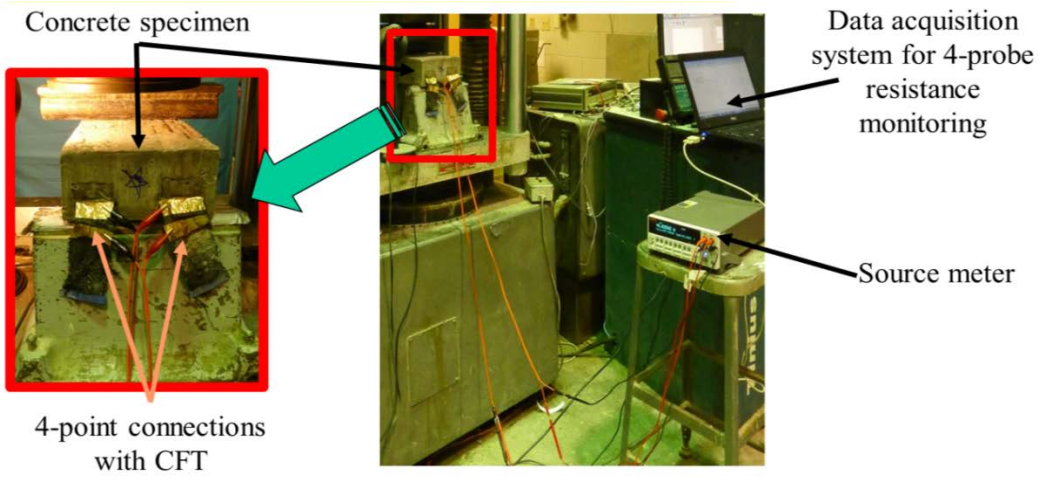

Figure 4.22 Resistance monitoring system

Figure 4.23 shows the complete setup used for the three- and four-point bending tests. Data related to force, deflection and resistance was acquired continuously during the tests. Figure 4.24 presents the three-point bending test on the Tinius Olsen machine, and Figure 4.25 describes the four-point bending test on the Tinius Olsen machine.

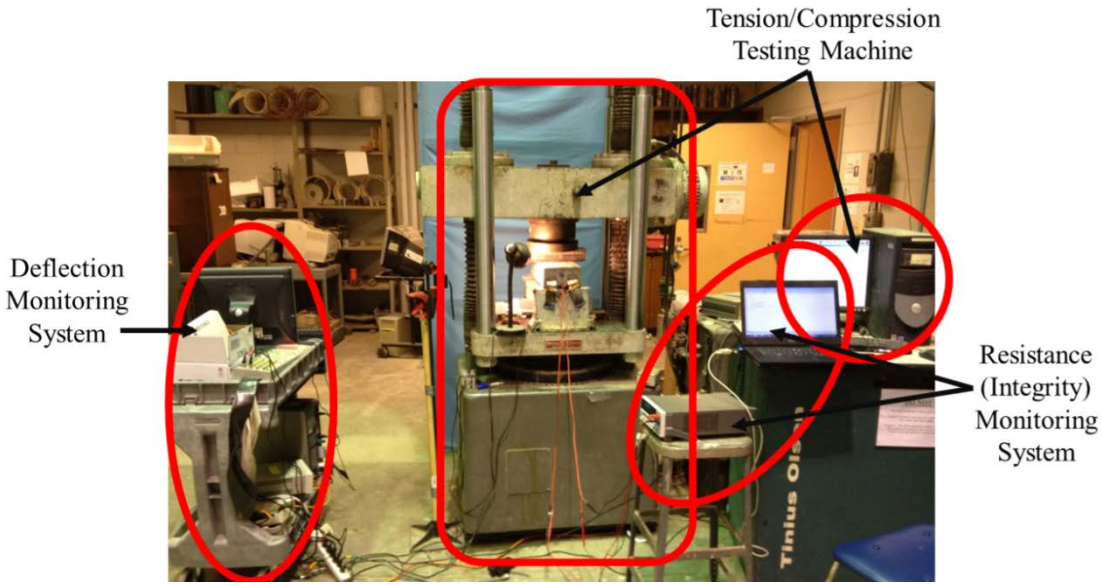

Figure 4.23 Test setup for the three- or four-point bending tests

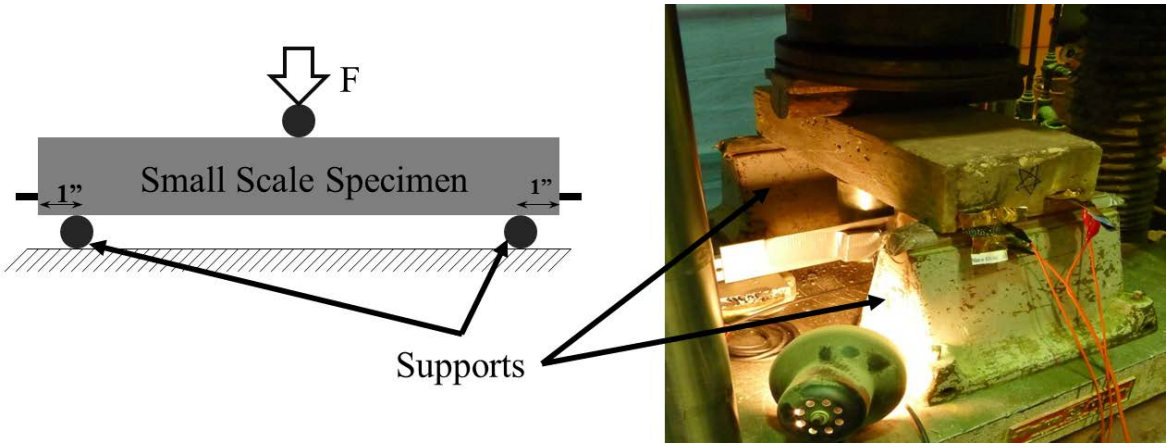

Figure 4.24 Three-point bending test schematic

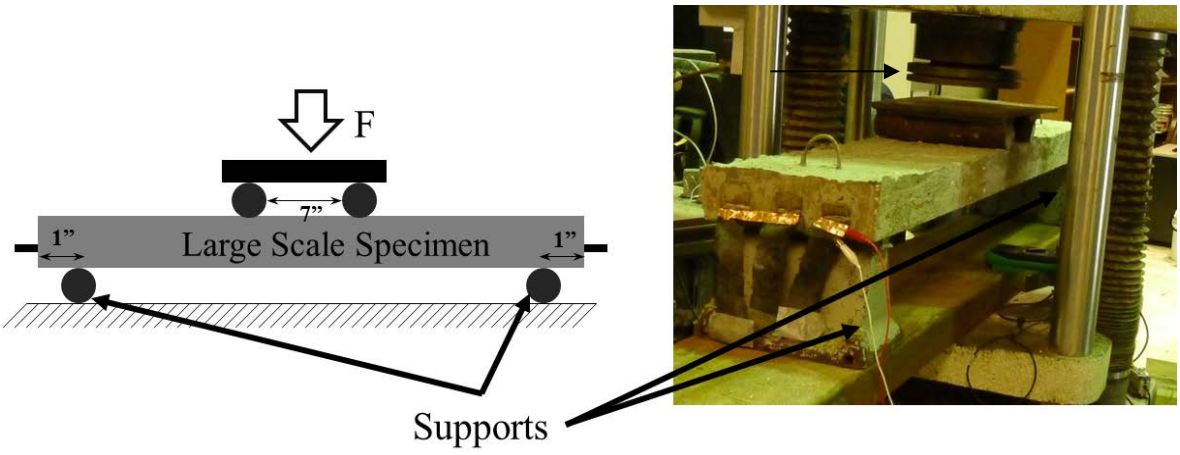

Figure 4.25 Four-point bending test schematic

4.4.3 Test Results and Discussions

Figure 4.26 and Figure 4.27 present the load-deflection curves obtained for the small-scale concrete specimen with rebars or CFTs, respectively. The reinforcement ratio for the specimen with CFT was 0.0008, while that for the specimen with rebar was 0.0158. Note the reinforcement ratio was based on the area of the reinforcement and strength difference in the CFT and steel rebars are not accounted for. The specimen with steel rebars ruptured at a defection of 0.55 in., or 14.0 mm, and that with the CFT broke at a deflection of 0.028 in., or 0.7 mm. This confirms that the CFT is much less ductile than steel rebar.

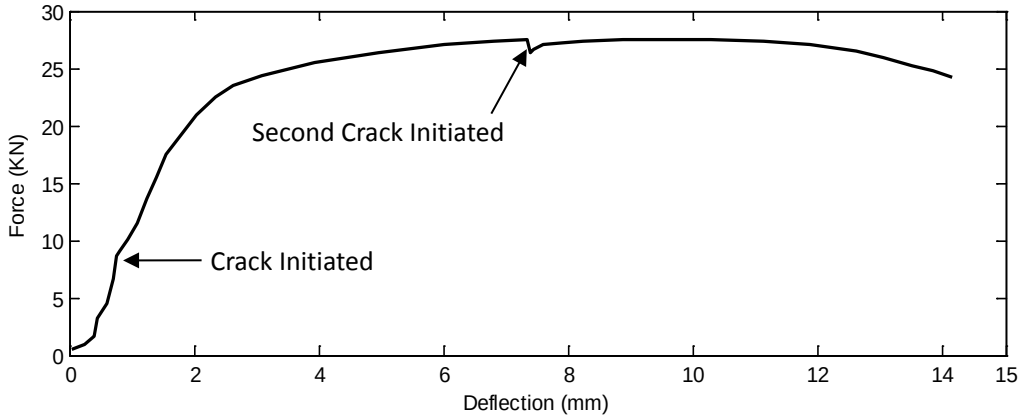

Figure 4.26 Load-deflection curve of steel rebar reinforced concrete slab from the three-point bending test

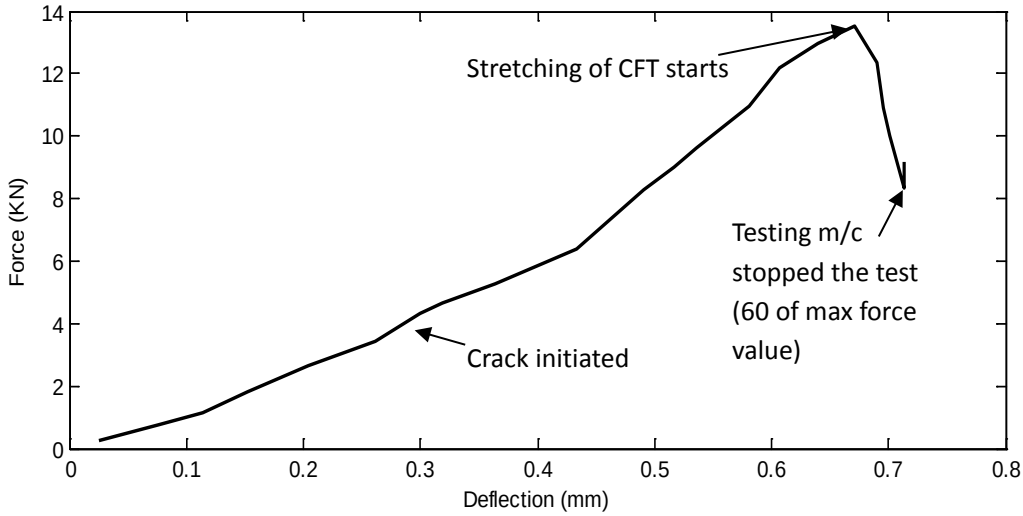

Figure 4.27 Load-deflection curve of the CFT reinforced concrete slab from the three-point bending test

Due to the 20 times smaller reinforcement ratio of the CFT specimen with respect to the steel rebar specimen, it is difficult to directly compare the effects of embedded CFT and steel rebar on the concrete slab flexural strength. To provide a direct comparison, load-deflection curves were normalized by referring to the technique presented by Chanvillard et al. (1990). As per the technique, the load (force) versus deflection curve presented in Figure 4.27 is re-plotted in Figure 4.28 as a function of the conditions when the first crack occurred. In other words, the values of force and deflection at first crack are assigned the values 1. Such a representation is convenient for assessing the residual strength of concrete specimen after the first sign of failure –

the first crack. This method also indicates that how much more load the structure can withstand after the first crack. As seen in Figure 4.28, use of the CFT as an embedded element may not provide the desired ductility, but it provides almost 20% more strength to the concrete slab compared to specimen embedded with steel rebars.

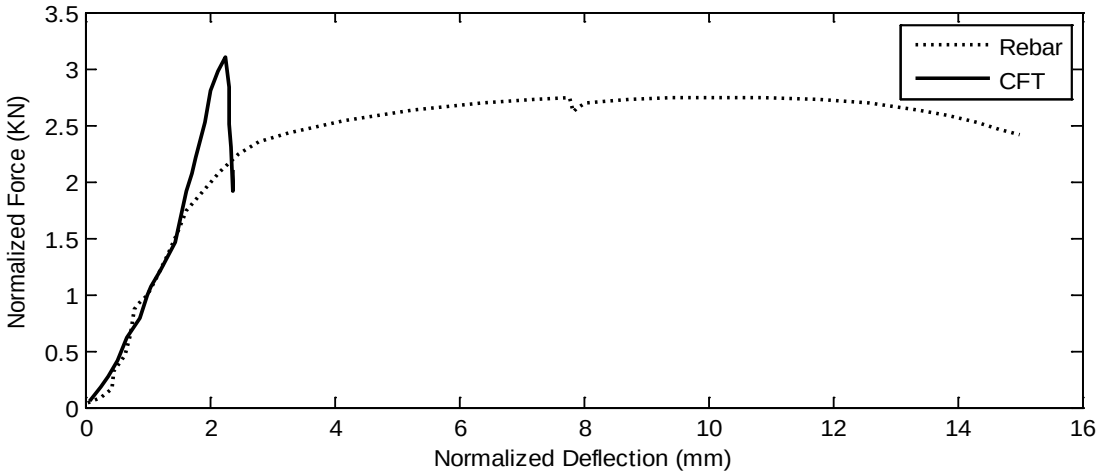

Figure 4.28 Normalized load-deflection curves for small-scale specimen embedded with steel rebar or CFT from the three-point bending test

Four-point bending test was conducted for the large-scale specimens and Figure 4.29 presents the load-deflection curves. The segmentation of the CFT curve is due to the safety feature of the Tinius Olsen machine. During the four-point bending test the specimens with CFTs, the first crack was followed by a sudden drop in force. Due to this sudden drop, a safety feature of the testing machine halted the test. A bending test was repeated on the same specimen to investigate its residual behavior. The response of the same specimen before and after the first crack is presented in Figure 4.29 and referred to as CFT1 and CFT2, respectively. Due to this abrupt shut down, the test had to be started from zero load and deflection values. As a result the response of specimen in CFT2 was very different than CFT1 and it is hard to join them together. Figure 4.29 clearly indicates that the CFT provides additional strength to the concrete prior to the cracking.

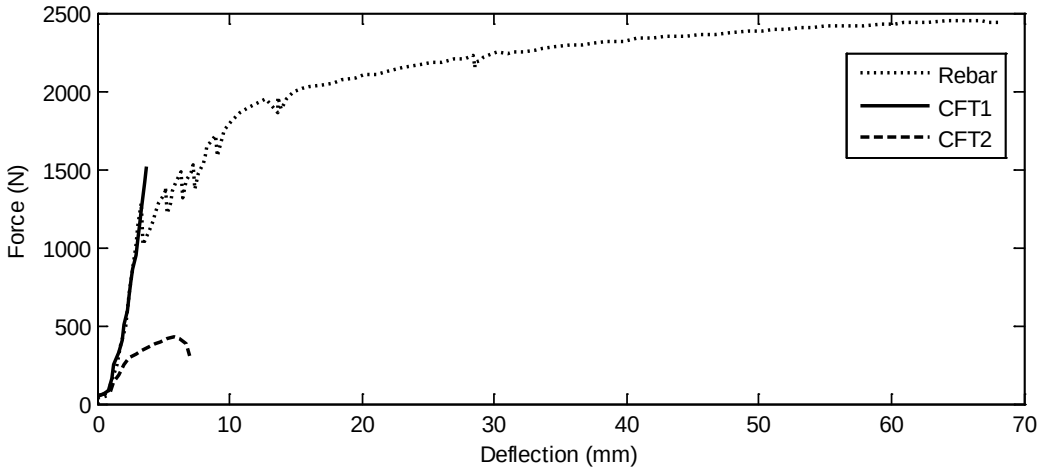

Figure 4.29 Load-deflection curve of concrete slab embedded with rebar or CFT from the four-point bending test

During the four-point bending test, the electrical resistance of the CFTs was continuously measured by the four-probe method. Figure 4.30 shows the variation of the electrical resistance of the CFT in response to the concrete slab deflection. Initial resistance data from CFT2 during reloading was omitted till the unloading point in CFT1 to obtain continuous resistance data. For reference, the load is also shown. Figure 4.30 shows a slight electrical resistance increase corresponding to the first crack for CFT1, indicating partial breaking of the carbon fibers in the CFT. When the CFT ruptures and the specimen fails in CFT2, the resistance increases abruptly, indicting a total breaking of carbon fibers in the CFT. The crack was estimated to be about 1/4 in. or 6 mm wide when the resistance of the CFT abruptly increases.

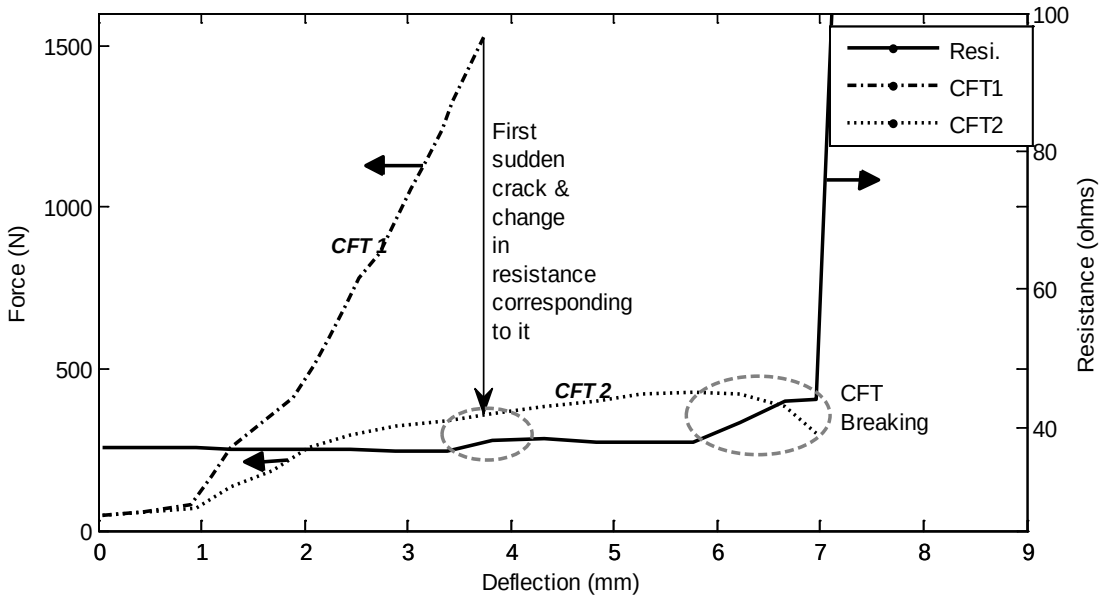

Figure 4.30 Electrical resistance of the CFTs in large-scale specimens during the four-point bending test

4.5 Summary

This chapter presents characterization of the CFT material and design, development and tests performed to investigate the effect of embedded CFT on the flexural behavior of concrete slabs. Several sets of tensile, pullout and bending tests were performed. For each test of specimen with CFT, a specimen of the same configuration with steel rebar was tested for comparison.

Material characterization tests show that the peak tensile force developed in the CFT is sensitive to strain or displacement rate, length of the specimen, and the clamping. While flexible coating such as silicone rubber epoxy allows slippage between the gripper and the CFT, rigid epoxy coating can improve clamping, allowing the CFT to develop much higher tensile force.

The pullout test results show that the strength of the bonding between concrete and CFT with or without silicone rubber epoxy coating exceeds the tensile strength of the CFT itself. Bending test results indicate that the CFT can provide higher strength to the concrete slab while being used as heating elements for deicing application. However the use of CFT alone for the reinforcement purpose is not recommended as the CFT can only provide very limited ductility as compared to steel rebar.

Bending test results show that the uncoated CFT can survive ¼ in. wide concrete crack without sacrificing its heating capacity. It is envisioned that the CFT coated with flexible epoxy can survive much large cracks in concrete slab.

CHAPTER 5: Field Performance of the CFT Heating Panel

5.1 Field Observation

The CFT heating panel was embedded in the concrete slab at the testing facility in September 2010 and it has been operating since then. During the 2010-2011 winter, the system was tested during intermittent deicing and anti-icing tests. This system was put on interrupted test during the entire 2011-2012 winter, when record snowfall (more than 133 in.) was recorded in Anchorage. After two winters' testing, the test sidewalk was careful examination and no apparent cracking was observed on the sidewalk surface, nor is there any disintegration of the concrete slab.

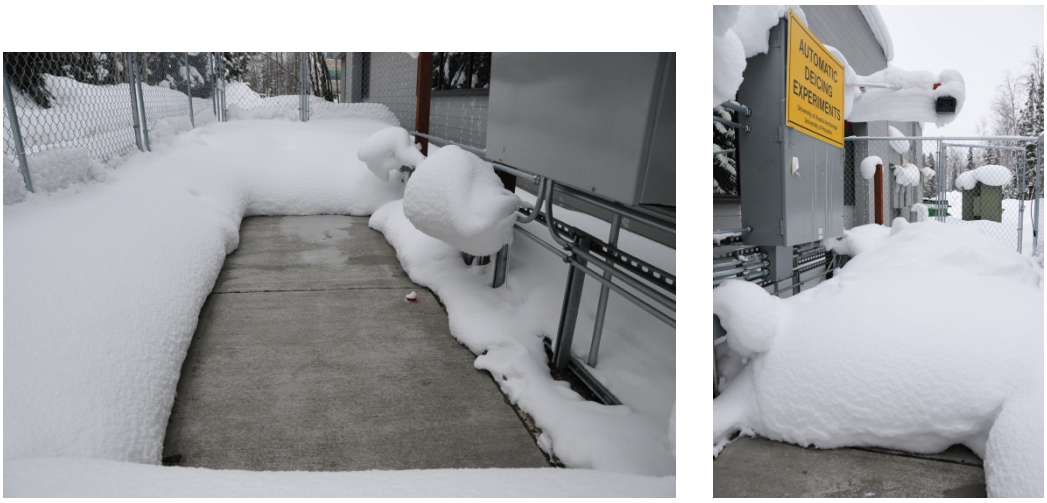

Figure 5.1 Snap shot of the test sidewalk with embedded CFT heating panels

5.2 Stability of the CFT Heating Panel Resistance

The deicing system worked very well in the two winter seasons of testing. During the last two winter seasona, the electrical resistances of the CFT heating panels were periodically measured by a handheld multimeter and Table 5.1 presents the resistance results along with air temperature. Figure 5.2 presents the variation of electrical resistance and air temperature with time. One can see from Figure 5.2 that the electrical resistance of the heating panels fluctuate between 0.8 to 1.4, exhibiting a rather stable electrical property. The fluctuation in resistance might be caused by the variation in moisture content, temperature, etc. Overall, it indicates that the heating panels, the power supply electrodes and the interface between the electrodes and the CFT's are quite stable.

Table 5.1 Measured electrical resistance of heating panels

Date	Block 2 (ohm)	Block 3 (ohm)	Block 4 (ohm)	Air Temp. (˚F)
09/16/2010	1.2	1.3	1.2	50
09/17/2010	1.1	1.1	1.1	48
09/24/2010	1.3	1.2	0.9	46
09/29/2010	1.1	1.1	0.9	40
10/04/2010	1.2	1.2	1	45
10/11/2010	1.2	1	0.9	37
10/14/2010	1.1	1	1	30
11/25/2010	1.1	1	0.9	32
12/01/2010	1	1	1	6
02/17/2011	0.9	1.1	1	12
04/17/2011	1	1	1	42
05/09/2011	0.9	1	0.9	50
07/03/2011	1	0.9	1.1	58
08/05/2011	1	0.8	0.9	56
09/07/2011	1.1	0.9	0.9	52
10/12/2011	1.1	1	0.9	34
11/01/2011	1.1	1	0.9	28
06/30/2012	0.8	0.8	0.85	57
07/03/2012	0.85	0.8	0.8	54
09/21/2012	0.95	0.95	0.95	50
11/06/2012	1.1	1.1	1.1	18
11/14/2012	1.1	1.2	1.1	26
11/19/2012	0.9	1.3	1.4	11
11/26/2012	0.9	-	-	8
12/03/2012	1.4	-	-	4
12/10/2012	1.0	1.0	0.9	26
12/18/2012	1.1	1.0	0.9	-1

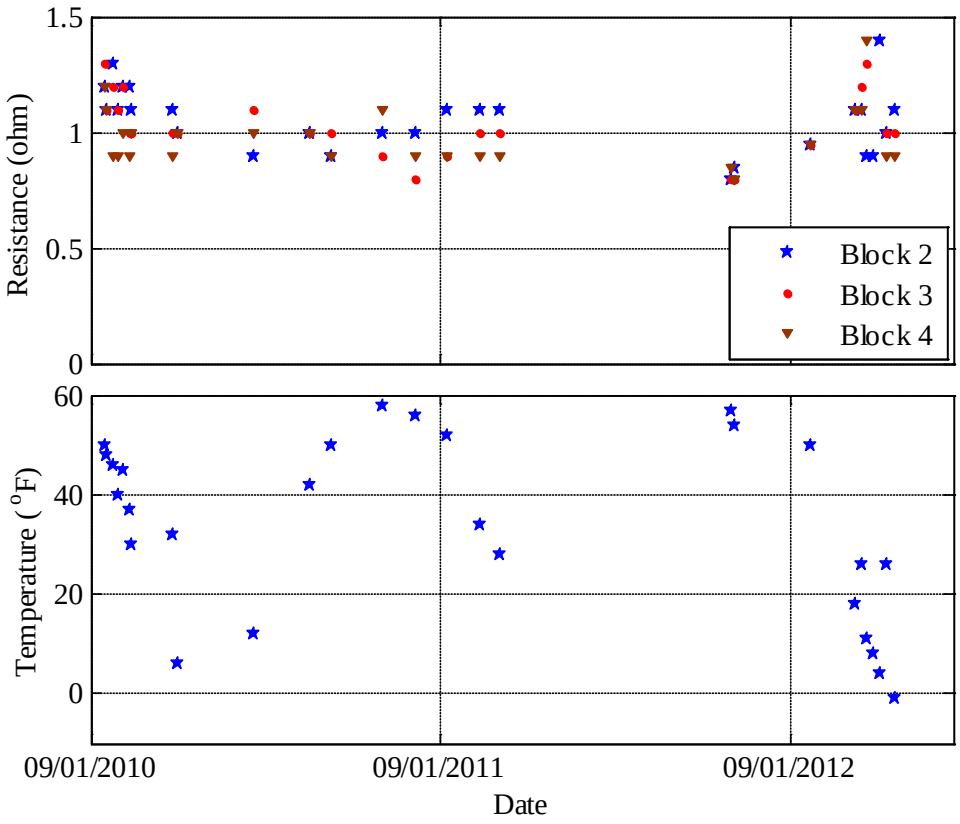

Figure 5.2. Temperature and electrical resistance variation with time

CHAPTER 6: Conclusions and Recommendation for Future Study

6.1 Conclusions

This report presents the results of a comprehensive study on the issues raised during the field experiment of the CFT heating panel embedded in concrete sidewalk for deicing. These issues include induced current, automatic control algorithms, impact of the CFT embedment on the structural integrity of concrete slabs, survivability of the CFT during concrete cracking, and field performance observation. Based on the study results, the following conclusions can be made:

1. The expected induced current in the steel rebar mesh is at the level of nano Amps, which is well below the current resolution of the instrument used to measure the induced current in the field. We believe it is negligible as long as corrosion is concerned.

2. Compared with the manual control, the ON/OFF automatic controller and advanced Fuzzy Logic-based automatic controller reduce the power consumption or cost by 59% and 70%, respectively. The ON/OFF controller is simple, efficient and easy to implement. It is recommended for field application.

3. Embedment of the CFT can provide higher strength to the concrete slab while being used as heating elements for deicing application. However use of the CFT alone for the reinforcement purpose is not recommended as the CFT can only provide very limited ductility as compared to steel rebar.

4. The uncoated CFT can survive ¼ in. wide concrete crack without sacrificing its heating capacity. It is envisioned that the CFT coated with flexible electrically insulating epoxy can survive much large cracks in concrete slab.

5. The CFT heating panel deicing system demonstrates excellent deicing/anti-icing capability and quite stable electrical resistance during the two and a half year long field trial. This shows the heating panel has a promising long term reliability and stability.

6.2 Future Study

Phase I of this project investigated the feasibility of the CFT heating panel in deicing applications. Phase II of this project focused on the survivability of the CFT heating panel to concrete slab cracking and its impact on the structural behavior of the concrete slab, along with control algorithms to improve its operating efficiency. Now this technology is ready to enter the

real world application from the laboratory. Continued experiments and observation of the test sidewalk is recommended to obtain data on the long-term performance of this system. One large-scale trial of this technology is deemed very necessary before its commercialization.

Reference

Bae, S.-W., Belarbi, A., and Myres, J. J., "Performance of Corrosion-Damaged RC Columns Repaired by CFRP Sheets," The 7th International Symposium on Fiber Reinforced Polymer Reinforcement for Reinforced Concrete Structures New Orleans, Louisiana, 2005.

Baumert, M. E., Green, M. F., Erki, M. A. (1996). “Low Temperature Behaviour of Concrete Beams Strengthened with FRP Sheets.” Proceedings of the 1996 CSCE Annual Conference, Edmonton, Alta. :179-190.

Birst, S., and Smadi, M. (2009). "Evaluation of North Dakota's Fixed Automated Spray Technology Systems," North Dakota State University, Fargo, ND.

Campbell-Allen, D. and Desai, P.M. (1967). “The Influence of Aggregate on the Behavior of Concrete at Elevated Temperature,” Nucl. Eng. and Design 6(1), 65–77.

Campbell-Allen, D., Low, E.W.E. and Roper, H. (1965). "An Investigation on the Effect of Elevated Temperatures on Concrete for Reactor Vessels," Nuclear Structural Engineering, Amsterdam, the Netherlands, 1 (2): 382-388

Chang, C., Ho, M., Song, G., Mo, Y.-L., and Li, H. (2009). "A Feasibility Study of Self-Heating Concrete Utilizing Carbon Nanofiber Heating Elements." Smart Material and Structures, 18(12).

Charpin, J. P. D., Myers, T. G., Fitt, A. D., Ballim, Y., and Patini, A. (2004). "Modeling Surface Heat Exchanges from a Concrete Block into the Environment." Mathematics in Industry.

Chanvillard, G., Banthia, N., and Aitcin, P.-C. (1990), "Normalized Load-Deflection Curves for Fibre Reinforced Concrete under Flexure," Cement & Concrete Composites, vol. 90.

Chen, J., and Li, W. (2003). "Application of fuzzy control PID algorithm in temperature controlling systems." 2nd International Conference on Machine Learning and Cybernetics, Henan, China, 4, 2601-2604.

Chiba, A., Kawazu, K., Nakano, O., Tamura, T., Yoshihara, S. and Sato, E. (1994). "The effects of magnetic fields on the corrosion of aluminum foil on sodium chloride solutions." Corrosion Science, 36(3): 539–543

Chung, D. D. L. (2004). "Self-heating structural materials." Smart Material and Structures, 13(3), 562-565.

Cox, J. V. and Cochran, K. B. (2003), "Bond between Carbon Fiber Reinforced Polymer Bars and Concrete. II: Computational Modeling," Journal of Composites for Construction, vol. 7, pp. 164-171.

Dai, J. G., Saito, Y., Ueda, T., and Sato, Y. (2005), "Static and Fatigue Bond Characteristics of Interfaces between CFRP Sheets and Frost Damage Experienced Concrete," in The 7th International Symposium on Fiber Reinforced Polymer Reinforcement for Reinforced Concrete Structures New Orleans, Louisiana.

Dong, Z., Su, Y., and Yan, X. (2009). "Temperature Control System of the Thermal Analyzer Based on Fuzzy PID Controller." Ninth International Conference on Hybrid Intelligent Systems, Shenyang, China.

Dutta, P. K. and Hui, D. (1996) “Low-temperature and freeze-thaw durability of thick composites.” Structural Composites in Infrastructures, Composites Part B: Engineering, v 27, n 3-4, 371-379.

Eckold, G. (1994) “Environmental Effects, Design and Manufacture of Composite Structure.” Woodhead Publishing Limited, 221-232

Grassi, E., and Tsakalis, K. (1996), "PID controller tuning by frequency loop-shaping." 35th IEEE Conference on Decision and Control, Kobe, Japan, 4776-4781.

Hassan, T. K. and Rizkalla, S. H. (2004), "Bond Mechanism of Near-Surface-Mounted Fiber-Reinforced Polymer Bars for Flexural Strengthening of Concrete Structures," Structural Journal, vol. 101, pp. 830-839.

He, S.-Z., Tan, S., Xu, F.-L., and Wang, P.-Z. (1993). "Fuzzy self-tuning of PID controllers." Fuzzy Sets and Systems, 56(1), 37-46.

Hou, Z. F., Li, Z. Q., and Tang, Z. Q. (2002). "Research on Making and Application of Carbon Fiber Electrically Concrete for Deicing and snow-melting." J. of Wuhan Institute of Technology (Natural Journal Edition). 24: 32-34.

Huang, S.-J., and Lo, Y.-h. (2009). "Metal Chamber Temperature control by Using Fuzzy PID Gain Auto-tuning strategy." WSEAS Transactions on Systems and Control, 4(1), 1-10.

Jackson, J. E., Lasseigne-Jackson, A. N. (2007). "The effect of magnetic fields on corrosion in pipeline steel." International Conference on Offshore Mechanics and Arctic Engineering, 2: 383-391

Jones, P. H., Jaffrey, B. A., Watler, P. K., and Hutchon, H. (1992). Environmental impact of road salting: Chemical deicers and the enviroment, Lewis Publishers, Chelsea, MI.

Kaiser, H. (1989). “Bewehren von staholeton mit kohlenstoffserver-starkten epoxiharzen.” Ph. D. Thesis, Diss ETH Nr. 8918. Empa, Zurich, Switzerland.

Kassir, M.K. Bandyopadhyay, K.K., and Reich, M. (1996). Thermal Degradation of Concrete in the Temperature Range from Ambient to 315°C (600°F). Brookhaven National Laboratory, Associated Universities, Inc., Upton, NY.

Kuemmel, D. E. (1994). "Managing Roadway Snow and Ice Control Operations."

Lee J.-K. and Lee J.-H. (2002), "Nondestructive evaluation on damage of carbon fiber sheet reinforced concrete," Composite Structures, vol. 58, pp. 139-147.

Li, H., Xiao, H., Ou, J., (2008). "Electrical property of cement-based composites filled with carbon black under long-term wet and loading condition." Composites Science and Technology. 68, 2114–2119.

Lorenzis, L. D., Nanni, A., and Tegola, A. L. (2000), "Strengthening of Reinforced Concrete Structures with Near Surface Mounted FRP Rods " in International Meeting on Composite Materials, PLAST2000 Milan, Italy.

Malvar, L. J., J. V. Cox, and K. B. Cochran (2003). "Bond between Carbon Fiber Reinforced Polymer Bars and Concrete. I: Experimental Study," Journal of Composites for Construction, vol. 7, pp. 154-163.

Mayo, R., Nanni, A., Watkins, S., Barker, M., and Boothby, T. (1999), "Strengthening of Bridge G-270 with externally bonded CFRP Sheets," Center for Infrastructure Engineering Studies, UMR, Rolla, MO.

Moon, U.-C., and Lee, K. Y. (2000), "Temperature control of glass melting furnace with fuzzy logic and conventional PI control." Proceedings of American Control Conference, Chicago, IL, USA, 2720-2724.

Mussato, B., Gepraegs, O., and Farnden, G. (2004). "Relative Effects of Sodium Chloride and Magnesium Chloride on Reinforced Concrete: State of the Art." Transportation Research Record, 1866`(8), 59-66.

Naus, D.J. (2005). The Effects of Elevated Temperature on Concrete Materials and Structures – a Literature Review. Oak Ridge National Laboratory, Report No. ORNL/TM-2005/553.

Ohkubo, K., Beppu, M., Ohno, T., and Satoh, K. (2008), "Experimental study on the effectiveness of fiber sheet reinforement on the explosive-resistant performance of concrete plates," International Journal of Impact Engineering, vol. 35, pp. 1702-1708,.

Okelo, R. and R. L. Yuan (2005). "Bond Strength of Fiber Reinforced Polymer Rebars in Normal Strength Concrete," Journal of Composites for Construction, vol. 9, pp. 203-213.

Osella, A., Favetto, A., and Lopez, E. (1998). “Currents induced by geomagnetic storms on buried pipelines as a cause of corrosion,” J. Applied Geophysics, 38 (3): 219-233.

Ramakrishnan, V. (2001). “Concrete plastic shrinkage-reduction potential of synergy fibers.” Transportation Research Record. 1775, Transportation Research Board, Washington, D.C., 106-117

Sasada, T. and Akira, S. (2000) "Convective corrosion pattern of steel in water under gradient magnetic fields." *Physics Letters A*, **266**(4-6): 350-358

Sato, A., Ogiwara, H., Miwa, T. and Nakabayashi, S. (2002) " Influence of high magnetic field on the corrosion of carbon steel." *IEEE Transactions on Applied Superconductivity*, **12**(1): 997 – 1000

Shahawy MA, Arockiasamy M, Beitelman T, Sowrirajan R. (1996a) “Experimental investigation on structural repair and strengthening of damaged prestressed concrete slabs utilizing externally-bonded carbon laminates.” Composites Part B 1996; 27: 217–24.

Shahawy MA, Arockiasamy M, Beitelman T, Sowrirajan R. (1996b) “Reinforced concrete rectangular beams strengthened with CFRP laminates.” Composites Part B 1996; 27: 225–33.

Sen, M. (2004). "A review of the principles and applications of thermal control." Journal of the Mexican Society of Mechanical Engineering, 1(4), 115-131.

Sueptitz, R., Tschulik, K., Uhlemann, M., Gebert, A. and Schultz, L. (2010) " Impact of magnetic field gradients on the free corrosion of iron. " *Electrochimica Acta*, **55**(18): 5200-5203

Sun, M., My, X., Wang, Z., Hou, Z., and Li, Z. (2008). "Experimental studies on the indoor electrical floor heating system with carbon black mortar slabs." Energy and Buildings, 40, 1094-1100.

Täljsten, B. and Elfgren, L. (2000). "Strengthening concrete beams for shear using CFRP-materials: evaluation of different application methods." Composites: Part B Engineering, 31 (2): 87–96

Tuan, C. (2004). "Electrical resistance heating of conductive concrete containing steel fibers and shavings." American Concrete Institute Materials Journal, 101(1), 65-70.

Visioli, A. (2001). "Tuning of PID controllers with fuzzy logic." Control Theory and Applications, 148(1), 1-8.

Wang, A. S. D. (1986). "On fracture mechanics of matrix cracking in composite laminate." Proc. Int. Symp. Composite Materials and Structure, Beijing, 576-584.

Ward, B. L. (2002). "Evaluation of a Fixed Anti-Icing Spray Technology (FAST) System." Paper presented at the 81st Annual Meeting of the Transportation Research Board, Washington, D.C., January 2002.

Wei, J. (2010). "Research on the Temperature Control System Based on Fuzzy Self-tuning PID." 2010 International Conference On Computer Design and Applications, Heibei, China.

Williams, D., Williams, N., and Cao, Y. (2000). "Road salt contamination of ground water in major metropolitan area and development of a biological index to monitor its impact." Water Research, 34(1), 127-138.

Yang, T., Yang, Z. J., Singla, M., Song, G., and Li, Q. (2012). "Experimental study on Carbon Fiber Tape-Based Deicing Technology." Journal of Cold Regions Engineering, 1-30.

Yehia, S., and Tuan, C. (1999). "Conductive concrete overlay for bridge deck deicing." American Concrete Institute Materials Journal, 96(3), 382-390.

Yehia, S., Tuan, C., Ferndon, D., and Chen, B. (2000). "Conductive concrete overlay for bridge deicing: Mixture proportioning, optimization, and properties." American Concrete Institute Materials Journal, 97(2), 172-181.

Yusof, R., Omatu, S., and Khalid, M. (1994), "Application of self-tuning PI(PID) controller to a temperature control system." 3rd IEEE Conference on Control Applications, Glasgow, UK, 1181-1186.

Zenewitz, J. A. (1977). “Survey of Alternatives to the Use of Chlorides for Highway Deicing.” *Rep. No.FHWA-RD-77-52*, U. S. Dept. of Transportation, Federal Highway Administration, Offices ofResearch and Development, Washington.

Zhang, Q. and Li, H (2011). “Experimental investigation of road snow-melting based on CNFP self-heating concrete.” Proceedings of SPIE, Behavior and Mechanics of Multifunctional Materials and Composites, vol. 7978,

Zhi, M., Xiaohong, P., and Laisheng, X. (2009). “Research and Application on Two-stage Fuzzy Temperature Control System for Industrial Heating Furnace.” 2009 Second International Conference on Intelligent Computation Technology and Automation, Changsha, China.

Zhou, K., and Yu, H. (2011). “Applicvation of fuzzy predictive-PID control in temperature control system of freeze-dryer for medicine material.” Second International Conference on Mechanic Automation and Control Engineering, Inner Mongolia, China.